Deep Insight in the Processes Occurring During Early Stages of the Formation and Room Temperature Evolution of the Core(Amorphous SiO_2)@Shell(Organocations) Nanoparticles

Sanja Bosnar†, Tatjana Antonić Jelić†, Josip Bronić†, Maja Dutour Sikirić‡, Suzana Šegota‡, Vida Čadež‡, Vilko Smrečki§, Ana Palčić† and Boris Subotić†*
†Laboratory for Synthesis of New Materials, Division of Materials Chemisty, Ruđer Bošković Institute, Bijenička 54, 10 000 Zagreb, Croatia
‡Laboratory for Biocolloids and Surface Chemistry, Division of Physical Chemisty, Ruđer Bošković Institute, Bijenička 54, 10 000 Zagreb, Croatia
§NMR Center, Ruđer Bošković Institute, Bijenička 54, 10 000 Zagreb, Croatia
*boris.subotic@irb.hr

ABSTRACT

Following the assumption that the crucial processes governing the formation, properties and evolution of the core(amorphous silica)@shell(organocations) nanoparticles take place during short-time, room-temperature (*rt*) stirring/aging of the homogeneous reaction mixtures (HmRMs) formed by hydrolysis of TEOS (tetraethyl orthosilicate) in solutions of $Org(OH)_n$, we investigated these processes by various experimental methods (pH, ionic conductivity, ^{29}Si-NMR, dynamic light scattering and atomic force microscopy). The analysis of the data obtained by detail and careful investigation of the "model" HmRMs having the starting chemical composition: $xTEOS:0.25TPAOH:20H_2O$ (TPAOH = tetrapropylammonium hydroxide; x = 0.05 – 1), offer some new elements for the understanding of the mechanisms of formation and *rt* evolution of the core@shell silica nanoparticles: (1) There is a resolute evidence of the formation of the stable, about 1.2 nm sized core(amorphous SiO_2)@shell(TPA^+ ions) nanoparticles below the critical aggregation concentration (CAC). (2) Due to the intensive particulate processes (growth, aggregation, disaggregation, dissolution) which take place during the *rt* aging of the investigated HmRMs, the equilibrated core@shell silica nanoparticles do not exist as individual primary ones, but as the aggregates (about 2 nm to about 20 nm), composed of 1 – 2 nm sized "primary" nanoparticles. (3) In spite of the most frequent meaning that the nanoparticle shell is composed of the "free" TPA^+ ions adsorbed on the surface of the nanoparticle core, the results of this study show that the nanoparticle shell can be formed mainly by attachment of the polysilicate anions (silicate oligomers), associated with TPA^+ ions, on the surfaces of the nanoparticles cores.

INTRODUCTION

Zeolites are crystalline silica or silica-alumina materials with periodic 3-D framework and well-defined microporous structure. Due to their unique properties such as acidity, porosity, and molecule-sieving ability, they have been widely used as catalysts, adsorbents, ion exchangers and micro-reactors in petroleum refining and fine chemical industry,[1-3] but also in electronic, optics, sensing and medicine[4]. The properties of zeolites, relevant for their different applications, are largely determined by their structural, chemical, particulate and morphological properties.[2, 5] Because the mentioned properties can be controlled by thorough understanding of the critical processes (nucleation, crystal growth) occurring during crystallization, the very complex processes, which at molecular level occur during crystallization of zeolites,[6] were in the focus of zeolite researchers since early days of zeolite synthesis.[7-9] Since then, many different approaches of the critical processes of zeolite crystallization (formation of hydrogel, nucleation, crystal growth) were established during the years of intense investigations.[4, 5, 10-17]

A new burst in the understanding of mechanism of zeolites crystallization happened at the end of 20th century and the beginning of 21st century, when several research groups reported formation of the stable, 2 – 5 nm sized, amorphous silica nanoparticles (amorphous precursor species – PPSs) in homogeneous systems (clear solution) SiO_2-TAAOH-AlkylOH-H_2O (TAA = tetraalkylammonium, AlkyOH = alkyl alcohol) at room temperature, formed by hydrolysis of TEOS (tetraethyl orthosilicate) in the systems, TEOS-TAAOH-H_2O.[18-23] It also has been found that the addition of Al into reaction mixture leads to the formation of the stable, nanosized aluminosilicate particles.[24-28] These findings provided an additional significance of these investigations by the fact that hydrothermal treatment of such homogeneous systems results in the formation of different nanosized zeolites,[18, 19, 23, 26-36] and in addition, that the sub-colloidal precursor

species (PPSs) have a crucial role at the early stage of crystallization of zeolites in heterogeneous systems (hydrogels).[37-42]

Following Iler's original ideas on silica nanoparticles[43] and knowing the possibility of the stabilization of silica by organic molecules,[44-46] several research groups suggested that the PPSs have a core@shell structure with amorphous silica at the core and organic molecules at the shell.[20-22, 23, 25, 33, 47-51] On the basis of numerous studies of the formation of silica nanoparticles in homogeneous systems, TEOS-$Org(OH)_n$-H_2O[20-23, 25, 28, 35, 47-56] [$Org(OH)_n$ is organic base, most frequently TAAOH (n = 1),[20, 22, 50] but also other organoammonium hydroxides[23, 27, 28, 50] were used as organic bases], it was concluded that silica-$Org(OH)_n$ solutions have well defined critical aggregation concentration (CAC) of silica for $OH^-/SiO_2 \approx 1$. Prior to this critical point (below the CAC; $OH^-/SiO_2 > 1$) no nanoparticles are detected in the solution.[20, 22, 25, 27, 28, 35, 49, 53-57] Namely, at the excess of OH^- ions below the CAC, all the $Si(OH)_4$ monomers, formed by hydrolysis of TEOS, are deprotonated[20-22, 25, 43, 49, 53, 55] and then, mutual reactions of the deprotonated monomers result in the formation of silicate oligomers.[20-22, 24, 25, 27, 28, 35, 47, 53-57] On the other hand, the $Si(OH)_4$ monomers formed above the CAC ($OH^-/SiO_2 < 1$), together with the dissolved oligomers and TAA^+ ions, are the possible building blocks of the nanoparticles.[20] The size of the inorganic core (SiO_2) is nearly independent on the diameter of the TAA^+ ion, but decreases with pH, suggesting that the electrostatic forces are a key factor controlling their size and stability.[20, 22, 32, 49, 55] The independence of the core size and shape upon changes in the cation size are good indications that the core is mostly cation free.[22] Hence it is reasonable to assume that the TAA-containing nanoparticle shell is formed by attachment of TAA^+ ions from solution to the surface of nanoparticle core.

In spite of enormous amount of the data obtained during these studies, and great contribution to the knowledge on the structure and properties of silica nanoparticles[18-25, 27, 28, 35, 41, 42,47-65] as well as in the understanding the mechanism of their formation,[22-25, 28, 35, 51-

[54, 66, 67] some inconsistencies and "grey zones" relating to the mechanism of nanoparticles formation (addition of silica monomers,[51] aggregation of oligomers,[54, 66] or both the mechanisms[67]), state of TAA^+ – especially TPA^+ ions in the nanoparticle shell and consequently, mode of formation and structure of nanoparticle shel,[20, 44-46, 49, 53, 55, 59, 60, 65] are still persisting in the published data. In addition, on the basis of the analysis of SAXS (Small-Angle X-ray Scattering) patterns of the nanoparticles formed above the CAC ($OH^-/SiO_2 < 1$), Fedeyko *et al*,[20] Eilertsen *et al*,[28] Rimer *et al*,[49] and Provis *et al*[51] concluded that the number density of nanoparticles increases, but their size remains nearly constant with decreasing ratio OH^-/SiO_2, at nearly constant pH. On the other hand, using the same method (SAXS), Yang and Navrotsky[21] concluded that both the number and size of nanoparticles increase with decreasing ratio OH^-/SiO_2. Finally, in spite of widely accepted thinking that silica nanoparticles can be formed only above the CAC,[20, 25, 27, 28, 35, 44, 45, 49, 51, 52, 54-57, 63] some results based on SAXS[21, 22] and DLS (Dynamic Light Scattering)[24, 53] measurements indicate that the silica nanoparticles can also be formed at, and below the CAC. Here, it must be noted that in most cases, the clear solutions (homogeneous reaction mixtures – HmRMs) were aged at room temperature for at least 12-24 h[22-25, 28, 33, 35, 49, 53, 55] and even longer[44, 52, 54] after the preparation and before the measuring of the characteristic values (pH, ionic conductivity, particle size, distribution of different LMW silicate species and oligomers in the liquid phase, connectivity of Si in oligomers and nanoparticles, etc.). Since it is our opinion that crucial processes governing the formation of PPSs take place during the hydrolysis of TEOS and immediately after the hydrolysis is finished (i.e., before the system is equilibrated), it is reasonable to assume that the observed inconsistencies and "grey zones" are caused by insufficiency of the knowledge on just the processes occurring at the early stage (time) of the PPSs formation. For this reason, pH and ionic conductivity of the investigated "model" HmRMs (IM-HmRMs) having the starting chemical composition: $xTEOS:0.25TPAOH:20H_2O$, were, in this paper, measured (collected) continuously at various times, after mixing of TEOS and TPAOH solutions,

while the other data (particle size distribution, AFM images, ^{29}Si-NMR) were collected at different times, after the entire amount of TEOS has been hydrolyzed (see Experimental methods). Then, the obtained data were used for the analysis of the mechanism of the nanoparticles (PPSs) formation and their evolution during room-temperature aging.

EXPERIMENTAL METHODS

Preparation of TEOS-TPAOH-H_2O systems

The investigated ("model") homogeneous reaction mixtures (IM-HmRMs) having the initial chemical compositions: xTEOS:0.25TPAOH:20H_2O (x = 0.05 – 1), were prepared at room temperature (*rt*) by adding the appropriate amounts of tetraethylorthosilicate (TEOS, Aldrich, 98 %, reagent grade) to a water solution of tetrapropylammonium hydroxide (TPAOH, 1M aqueous solution, Alfa Aesar). For this purpose, the appropriate amount (mass) of TPAOH solution was added into plastic vessel containing appropriate amount (mass) of deionized water stirred by magnetic bar. Then, the appropriate amount (mass) of TEOS was quickly added to the stirred TPAOH solution. The moment of addition of TEOS into TPAOH solution was taken as the zero time**,** (t_s = 0) of the stirring/aging processes. Then, such prepared reaction mixtures were stirred at *rt* for time t_s and/or additionally aged at *rt*, under static conditions, for time t_a. If not defined otherwise, $t_s + t_a$ = 1440 min if t_s and t_a are expressed in minutes, or $t_s + t_a$ = 24 h if t_s and t_a are expressed in hours. The treatment of the reaction mixtures during and after stirring and/or after additional aging was conformed to the experimental method used for characterization (see below).

Characterization

^{29}Si NMR experiments were carried out on a Bruker Avance 600 spectrometer (600,13 MHz, ^{1}H; 119,22 MHz, ^{29}Si). The samples of IM-HmRMs with x = 0.1, 0.2, 0.25, 0.3, 0.5, 0.75 and 1.0 were prepared in the way described above, and then, the samples were transferred into 5 mm NMR tubes after; (i) *rt* stirring for t_s = 3 h**.** and (ii) additional

rt aging under static condition for t_a = 21 h (t_s + t_a = 24 h). Typically, spectra at a spectral width of 50 kHz and a digital resolution of 1.5 Hz per point were measured with 512 scans. A 30° pulse was used with a repetition rate of 7 s. All experimental data were zero-filled to double the number of experimental points. The software TopSpin (Bruker BioSpin) version 2.1 was used for all acquisition and processing. ^{29}Si NMR quantification was performed by spectral deconvolution using the Dmfit software.[68]

The pH and ionic conductivity of the IM-HmRMs with x = 0.05, 0.1, 0.125, 0.15, 0.175, 0.2, 0.22, 0.25, 0.35, 0.5, 0.75 and 1.0 were measured under stirring at *rt*, in the vessels in which the reaction mixtures have been prepared. For this purpose, pH electrode or conductivity cell was immersed into stirred solution (reaction mixture), about 1.5 min after addition of TEOS into TPAOH solution. Then, pH was continuously recorded at various times t_s (t_s is the time of stirring) from $t_s \approx$ 1.5 min to t_s = 50 – 70 min, at which the measuring of pH was stopped. On the other hand, due to high starting alkalinity of the investigated IM-HmRMs (pH > 13.6), the conductivity cell was, between two consecutive recording of conductivity, pulled out from the vessel with IM-HmRM, rinsed with deionized water and deleted (dried) with filter paper. Depending on x, the last value of the ionic conductivity of the IM-HmRMs were recorded at at t_s = 50 – 76 min. The samples remaining after the continuous measuring of pH and ionic conductivity, respectively, were additionally aged at *rt* for a given time t_a, so that t_s + t_a = 1440 min (24 h) and then, pH and ionic conductivity, respectively, were measured in the additionally aged samples. The values of *S* (ionic conductivity), presented in Fig. 3 and the values of pH, presented in Fig. S4, represent the average values of the results obtained by measuring in five independently prepared IM-HmRMs.

The pH of the IM-HmRMs was measured using a Corning Pinnacle 555 pH/ion meter. The pH meter was calibrated with pH 9.0 and 12.0 buffer solutions at 25 °C. The accuracy of the pH meter was ±0.01 pH units.

The ionic conductivity of the IM-HmRMs was measured using a Metrohm 712 Conductometer. The Conductometer was calibrated with KCl standard.

The size distribution of the nanoparticles formed/present in the IM-HmRMs was determined by means dynamic light scattering (DLS), using a photon correlator spectrophotometer equipped with a 532 nm "green" laser (Zetasizer Nano ZS, Malvern Instruments, UK). Intensity of scattered light was detected at the angle of 173°. To avoid overestimation arising from the scattering of larger particles, the hydrodynamic diameter (D_h) was obtained as a value at peak maximum of size number distribution function. The samples of the IM-HmRMs with x = 0 (0.694 M solution of TPAOH), 0.05, 0.1, 0.15, 0.2, 0.25, 0.275, 0.35, 0.5, 0.65, 0.75 and 1.0, used for DLS measurements, were prepared by the way described in previous section and stirred for the time, t_s, and/or additionally aged under static for the time $t_a = 24 - t_s$ (in hours), before the measurement. Each sample was measured 10 times and the results were expressed as the average value. All measurements were conducted at 25 ± 0.1 °C. The data processing was done by Zetasizer software 6.32 (Malvern instruments).

AFM imaging of the nanoparticles present in the investigated systems was performed in soft tapping mode using a MultiMode Scanning Probe Microscope with a Nanoscope IIIa controller (Bruker, Billerica, USA) with a vertical engagement (JV) 125 mm scanner. For this purpose, 5 μL of each of the selected IM-HmRMs (x = 0, 0.1, 0.2 and 1.0; t_s = 3 h and $t_s + t_a$ = 24 h, respectively), prepared as described in previous section, was pipetted directly onto mica substrate and incubated for 10 min. Then, the excess of the IM-HmRM was removed from the substrate by filter paper and the mica sheets were placed in enclosed Petri dishes for several hours at a relative humidity of up to 50% to evaporate the excess water. Processing and analysis of images were carried out using the NanoScopeTM software (Digital Instruments, Version 5.12r5, Digital Instruments, Tonawanda, NY, USA). All images are presented as raw data except for the first-order two-dimensional flattening. The NanoScope was allowed to equilibrate thermally for 1 h

before imaging. Scanning rates were normally optimized around 1 Hz at a scan angle of 90°. Images were recorded under ambient conditions in air, by using silicon tips (RTESP, Bruker, nom. freq. 320 nom. freq. 320 kHz, nom. spring constant of 42 Nm1). Images were processed and analyzed by means of the offline AFM NanoScope.

RESULTS AND DISCUSSION

As already has been pointed out in the Introduction, the entire amount of silica, formed by hydrolysis of TEOS exists as a mixture of monomers and oligomers below the critical aggregation concentration (CAC) of silica, and as a mixture of monomers, oligomers and nanoparticles above the CAC.[20-22, 24, 25, 27, 28, 44, 45, 49, 51-57] Identification of different silicate species (monomers, oligomers, nanoparticles) and Si-O-Si connectivity (expressed as Q^n, where n is number of bridging oxygen atoms per SiO_4) in the TEOS-$Org(OH)_n$-H_2O homogeneous reaction mixtures (HmRMs – clear solutions) were most frequently realized by ^{29}Si-NMR spectroscopy.[24, 27, 28, 35, 43, 44, 52, 54, 56, 57]

Figure 1 shows the ^{29}Si-NMR spectra of the investigated "model" homogeneous reaction mixtures, obtained by room-temperature hydrolysis of TEOS and aging of the reaction mixtures having the initial molar compositions: xTEOS:0.25TPAOH:20H_2O (IM-HmRMs in the further text; see Experimental methods). The ^{29}Si-NMR spectra were measured after t_s = 3 h (Fig. 1A) and after $t_s + t_a$ = 24 h (Fig. 1B); here, t_s is the time of the room-temperature (*rt*) stirring of the IM-HmRMs and t_a = 21 h is the time of the additional *rt* aging of the IM-HmRMs under static conditions (without stirring; see Experimental methods). Presence of only sharp lines, characteristic for dissolved silicate oligomers below the CAC (x < 0.25) and the appearance of broader bands above the CAC (x > 0.25), are consistent with the results of previous studies.[24, 27, 28, 35, 54, 57] Consequently, the distribution of Si between oligomers and nanoparticles (see Figs. S1Aa and S1Ba in the Supporting Information SI-1), types of oligomers and their distributions (Figs. 2Aa and 2Ba) as well as connectivity of the Si atoms in the silicate species distributed in the

clear solutions, investigated in this work (Figs. S1Ab and S1Bb in SI-1), are also in large extent consistent with the results of the corresponding previous studies.[27, 28, 54, 57]

For this reason, the distributions of oligomers (Figs. 2Aa, 2Ba, S1Aa and S1Ba) and their Q^n values (Figs. S1Ab and S1Bb) in the IM-HmRMs are not discussed here, but in SI-1, taking into consideration known relationships between the chemical composition of TEOS-Org$(OH)_n$-H_2O reaction mixtures and the distribution of oligomers and their Q^n values.[22,24,25,27,28,47,55,58,59,60,61,65,67] However, for the sake of further discussion, here must be emphasized that; (i) the near constancy of the amounts of Si in monomers (M), dimers (D) and cyclic trimers (3R) for x = 0.1 (below the CAC), in the time interval from t_s = 3 h (Fig. 2Aa) to $t_s + t_a$ = 24 h (Fig. 2Ba; see details in SI-2) indicates that the silicate exchange in alkaline aqueous solutions are rapid processes and thus, that the distribution of silicate monomers and oligomers measured at t_s = 3 h (Fig. 2Aa) is established earlier, e.g., at t_s < 3 h, (ii) although above the CAC (x ≥ 0.3), amounts of Si in M (○), D (●) and 3R (△) are comparable for t_s = 3 h (Fig. 2Aa) and $t_s + t_a$ = 24 h (Fig. 2Ba), the amounts of Si in 4R (▲), D3R (□) and D4R+D5R (■) are higher at t_s = 3 h (Fig. 2Aa) than at $t_s + t_a$ = 24 h (Fig. 2Ba) and (iii) in difference to expected domination of the Q^3 sites in the nanoparticles for each value of x at $t_s + t_a$ = 24 h[27, 28, 54, 55] (Fig. 2Bb), the ratio Si-Q^3/Si-Q^4 is close to 1 for all the measured values of x at t_s = 3 h (Fig. 2Ab). The observations indicated in (ii) and (iii) are closely related and will be discussed and explained further in the paper.

Measuring of ionic conductivity and pH are widely used for determination of the critical aggregation concentration (CAC) of silica in the TEOS-Org$(OH)_n$-H_2O HmRMs. However, while the conductivity, *S*, and pH were usually measured after longer *rt* aging (12 – 24 h or longer; see Introduction[22,25, 49, 53, 55]), the values of *S* and pH were, in this work, measured continuously during hydrolysis of TEOS and additional *rt* aging of the IM-HmRMs (see Experimental methods). Figure 3 shows that ionic conductivity, $S_{x,t}$, is almost constant ($S_{x,t} \approx S_{x,0}$ = 48.8 mS/cm, which corresponds to 0.7 M TPAOH solution;

0.25TPAOH:20H_2O) or slightly decreases during the first 5 – 7 minutes of stirring. Thereafter the values of $S_{x,t}$ rapidly decrease until reaching approximately constant (equilibrium) value, $S_{x,t} = S_{x,eq}$ at the time, $t_s = t_{eq}$ and to the value $S_{x,t} = S_{x,24h}$ at $t_s + t_a = 24$ h, respectively (see Fig. 3 and Table 1). Here, $t_a = 24 - t_{eq}$ is the time (in hours) of additional *rt* aging of the IM-HmRMs (after stirring), under static condition (see Experimental methods).

The initial rapid linear decrease of both $S_{x,m} = S_{x,eq}$ and $S_{x,m} = S_{x,24h}$ (solid straight lines in Fig. 4A), followed by the slow decrease of both $S_{x,m} = S_{x,eq}$ and $S_{x,m} = S_{x,24h}$ (dashed straight lines in Fig. 4B), are consistent with the results of previous studies.[20, 22, 25, 49, 53, 55] Here must be noted that the value of $[SiO_2]_{x,tot}$ in Fig. 4 represents the molality concentration of the SiO_2 formed by complete hydrolysis of TEOS and thus, $[SiO_2]_{x,tot} = [TEOS]_{x,0}$ is proportional to x (see Table 1), where $[TEOS]_{x,0}$ is the starting molality concentration of TEOS at $t_s = 0$.

Figure 5 shows the changes of the molality concentrations, $[OH^-]_{x,t}$, of OH^- ions during *rt* preparation and aging (with stirring) of the IM-HmRMs. The concentrations $[OH^-]_{x,t}$ are calculated by the relation: $[OH^-]_{x,t} = 10^{(14-pH)}$, from the corresponding values of $pH = pH_{x,t}$ (Fig. S4 in SI-2), measured as it is described in the Experimental methods, and corrected by the method described in SI-2. The change of the concentration, $[OH^-]_{x,t}$, is characterized by its initial slow decrease, whereupon the value of $[OH^-]_{x,t}$ changes with a higher, but decreasing rate till the "breakthrough" time, $t_s = t_b$. The "breakthrough" time $t_s = t_b$ is characterized by the intersections of the solid and the dashed curves (see Figs. 5a and 5b), in which the concentration of OH^- ions reaches the specific (pseudo-equilibrium) value, i.e., $[OH^-]_{x,t} = [OH^-]_{x,b}$.

From previous studies[20-22, 25, 49, 53, 55] and the relationships expressed by Eqs. (S2) and (S3) in SI-2, it is evident that the changes in conductivity and concentration of OH^- ions, below the CAC, can be rationalized on the basis of the acid-base chemistry of silicic acid and silica oligomers. Both the conductivity and concentration of OH^- ions drop

because the consumption of OH^- ions for deprotonation of the silica monomers formed during hydrolysis of TEOS [see Eqs (S2) and (S3) in SI-2]. On the basis of Eq. (S2), it is evident that the rate, $d[OH^-]_{x,t}/dt_A$, of the consumption of OH^- ions for deprotonation, is proportional to the product of the concentration, $[OH^-]_{x,t}$, of free (unspent) OH^- ions and the concentration, $[Si(OH)_4]_{x,t} = [SiO_2]_{x,t}$, of the $Si(OH)_4$ monomers at any stirring (aging) time, t_s i.e.,

$$d[OH^-]_{x,t}/dt_s = -k_1 \times [OH^-]_{x,t} \times [SiO_2]_{x,t} \quad (1)$$

Since $[SiO_2]_{x,t} = [TEOS]_{x,S,t}$, where $[TEOS]_{x,S,t} = [TEOS]_{x,0} - [TEOS]_{x,t}$ is the amount (molality concentration) of the TEOS, hydrolyzed and spent for the formation of $Si(OH)_4$ and other silica species (oligomers below the CAC and nanoparticles above the CAC), and $[TEOS]_{x,t}$ is the amount (molality concentration) of the non-hydrolyzed TEOS at time $t_s > 0$, Eq. (1) can be rewritten in the form,

$$d[OH^-]_{x,t}/dt_s = -k_1 \times [OH^-]_{x,t} \times \{[TEOS]_{x,0} - [TEOS]_{x,t}\} \quad (2)$$

On the other hand, Matsoukas and Gulari[58] observed that in the systems of high water content, such as those of interest here, hydrolysis is relatively fast process, largely independent of water concentration and pseudo-first-order in the concentration, $[TEOS]_{x,t}$, of the non-hydrolyzed TEOS, i.e.,

$$d[TEOS]_{x,t}/dt_s = -k_2 \times [TEOS]_{x,t} \quad (3)$$

On the basis of these findings, the changes of $[OH^-]_{x,t}$, and $[TEOS]_{x,t}$ during *rt* stirring of the IM- HmRMs, were calculated by simultaneous numerical solutions of the differential equations (2) and (3) using a fourth-order Runge-Kutta method and corresponding

numerical values of appropriate constants and initial conditions, as explained in the Supporting Information SI-3.

Almost perfect agreement of the measured values of $[OH^-]_{x,t}$ (symbol ○ in Fig. 5) and the values of $[OH^-]_{x,t}$ calculated by simultaneous numerical solutions of the equations (2) and (3) (solid curves in Fig. 5) in the time interval from $t_s = 0$ to $t_s = t_b$ shows that Eqs. (2) and (3) satisfactorily describe the relevant processes (hydrolysis of TEOS and deprotonation of the $Si(OH)_4$ monomers formed during hydrolysis of TEOS) occurring in the mentioned time interval. Since the backward reaction (protonation of the $Si(OH)_3O^-$ monomers and other deprotonated silicate species) is not included in Eq. (2), the agreement between measured and calculated values of $[OH^-]_{x,t}$ shows that the effect of the backward reaction on the concentration of OH^- ions is negligible at least to $t_s \approx t_b$. On the other hand, a sudden achieving of the pseudo-equilibrium concentration, $[OH^-]_{x,t} = [OH^-]_{x,b}$, at $t_s = t_b$ (see Fig. 5) indicates that at this point the rate of forward reaction (deprotonation) considerably decreases and approaches to the rate of the backward reaction. This is, at the same time, the reason that the measured (symbol ○ in Fig. 5) and calculated (solid curves in Fig. 5) values of $[OH^-]_{x,t}$ starts to differ at $t_s = t_b$ and that the difference between the measured and calculated values of $[OH^-]_{x,t}$ increases with time t_s. However, a slow decrease of the concentration of OH^- ions from $[OH^-]_{x,t} = [OH^-]_{x,b}$ at $t_s = t_b$ to $[OH^-]_{x,t} = [OH^-]_{x,24h}$ at $t_s + t_a = 24$ h (see Fig. 4), indicates that the rate of the backward reaction (protonation) does not surpass the rate of the forward reaction (deprotonation), at least to $t_s + t_a = 24$ h. As it can be expected from the results of previous studies,[20, 22, 25, 49, 53, 55] the values of $[OH^-]_{x,n}$ linearly decrease with the increasing concentration, $[SiO_2]_{x,tot}$ to $[SiO_2]_{x,tot} = [SiO_2]_{x,tot,b} \approx 0.6$ mol/kg for n = b and to $[SiO_2]_{x,tot} = [SiO_2]_{x,tot,24h} \approx 0.56$ mol/kg for n = 24 h. Thereafter, the values of $[OH^-]_{x,n}$ very slowly changes (decreases) with further increase of $[SiO_2]_{x,tot}$ (Fig. 4).

Analyzes of the data presented in Table 1 and Figs. 4 and 5 (see SI-4) lead to an assumption that the rate of formation of $Si(OH)_4$ monomers [see Eq. (S1) in SI-2] is

higher than the rate of their deprotonation [see Eqs. (S2) and (S3) in SI-2] and thus, that the ratio $[OH^-]_{x,S,t}/[SiO_2]_{x,t}$ is lower than 1 during the hydrolysis of TEOS. This assumption is consistent with the previous postulations that "…TEOS hydrolysis is rapid compared to all other processes...,"[59] and thus that "...after a short period of time the mixture contains silicic acid ($Si(OH)_4$), ethanol (EtOH), water, TPA cations and OH anions".[51, 53] The slow initial decrease of both the ionic conductivity $S_{x,t}$ (Fig. 3) and the concentration, $[OH^-]_{x,t}$, of the OH^- ions (see Fig. 5) also corroborate this assumption. To prove (or disapprove) this assumption, the values of $[SiO_2]_{x,t}$ and $[OH^-]_{x,S,t}$ were calculated by simultaneous numerical solutions of the differential equations (2) and (3) and then, the calculated ratios $[OH^-]_{x,S,t}/[SiO_2]_{x,t}$ were compared with the measured ratios $[OH^-]_{x,S,t}/[SiO_2]_{x,t}$. The obtained results (see Fig. 6) show that the calculated ratios $[OH^-]_{x,S,t}/[SiO_2]_{x,t}$ (solid curves) continuously increase from 0 at $t_s = 0$ to > 0 at the final time ($t_s = 75$ min) used in the analysis, but that for all the analyzed cases, the measured ratios $[OH^-]_{x,S,t}/[SiO_2]_{x,t}$ (symbol ○ in Fig. 6) are lower than 1 in the time interval from $t_s = 0$ to $t_s = 75$ min. In addition the last two columns in Table S5 in SI-4 show that the measured values of $[OH^-]_{x,S,t}/[SiO_2]_{x,t}$ are lower than 1 at even $t_s + t_a = 24$ h. Hence, it is evident that the rate of deprotonation of $Si(OH)_4$ monomers [Eqs. (S2) and (S3) in SI-2] is slower than the rate of their formation by hydrolysis of TEOS [(Eq. (S1) in SI-2] and thus, that a certain amount of free $Si(OH)_4$ monomers is present in the investigated IM-HmRMs not only above the CAC, but also below the CAC. From the data in Fig. 6 it can be calculated (see SI-4) that the molar ratio $[Si(OH)_4]_{x,t}/[\text{deprotonated monomers and oligomers}]_{x,t} \approx 40$ at $t_s = 1$ min, and that the same ratio is about 8 at $t_s = 5$ min. Hence, knowing that the presence of $Si(OH)_4$ monomers is crucial for the formation of silica nanoparticles,[20, 22, 51, 55, 58-61] it is reasonable to assume that, in spite of a widely spread opinion that the formation of silica nanoparticles starts to occur above the CAC,[20-22, 24, 25, 27, 28, 35, 44, 45, 49, 51, 53-57] the silica nanoparticles can also be formed at the early stage of TEOS hydrolysis and thus, below the CAC. The nanoparticles are not observed in the corresponding ^{29}Si-NMR

spectra for x ≤ 0.25 (see Fig. 1 as well as Figs. S1Aa and S1Ba in SI-1), which is consistent with the results of previous studies.[24, 27, 28, 35, 54, 56, 57] The most possible reason is very small amount (fraction) of silica present in eventually formed nanoparticles, which is below the detection limit of the applied method (see Experimental section). On the other hand, since DLS detects the presence of nanoparticles earlier than any other method,[24] selected reaction mixtures, stirred/aged at room temperature for the determined times, were analyzed by DLS and, additionally by AFM.

The DLS analysis of SiO_2-free "reaction mixture" 0.25TPAOH:20H_2O (0.694 M solution of TPAOH) does not show the presence of the "particles" having the size (diameter) $D \geq 1$ nm (see Fig. 7A and Table S6 in SI-5). On the basis of the analysis presented in SI-5 and the AFM images of the "blank sample" (0.694 M solution of TPAOH; see Fig. S9), it is reasonale to assume that the features having the size $D \geq 1$ probably corresponds to the hydrated TPA^+ ions. Addition of SiO_2 in the reaction mixture (by hydrolysis of TEOS for t_s = 3 h), even in minimum amount (x = 0.05, see Table 1), causes the formation of the features having the size (diameter) $D \geq 1$ nm (see solid curves in Fig. 7 and the data in Table S6 in SI-5). On the basis of the analysis presented in SI-5, it is concluded that the features having the size $D \geq 1$ nm represent the silica nanoparticles, and that the the presence of small silicate oligomers, even larger ones, does not considerably participate in the population of particles with $D \geq 1$ nm. Here it is interesting that the average size, $D_{av(\geq 1nm)}$, of these nanoparticles is constant (≈ 1.2 nm; see Table S6 in SI-5) to x ≤ 0.275 and close to the peak sizes (D_p = 1.25 – 1.35 nm) of the discrete particles populations identified in the corresponding DLS-PSD curves by intensity (see Figs. S8Ac, S8Ad, S8Bc and S8Bd in SI-5). A linear increase of the relative number, $N_{np}(rel) = N_{(D \geq 1\ nm)}$, of these nanoparticles with the amount, $[SiO_2]_{x,tot} \propto x$ (see Table S6 and Fig. S7A in SI-5), leads to the reasonable assumption that the formation of nanoparticles below the CAC (0 < x ≤ 0.25) takes place by addition or removal of monomeric units, i.e., by the mechanism which has previously been suggested for the

formation of nanoparticles above the CAC.[51] On the other hand, the average size, $D_{av(\geq 1nm)}$ ≈ 1.2 nm (see Table S6 in SI-5) of the nanoparticles formed below the CAC is comparable with the size, D < 1.5 nm, calculated on the basis of one-step simulation procedure (silica polymerization from a random initial conditions without any pre-association with organic structure directing agents - OSDAs), using Monte Carlo method.[59] Hence, it is reasonable to conclude that, below the CAC, the nanoparticles form by polymerization via addition of $Si(OH)_4$ monomers which are not pre-associated with OSDAs. This explains the linear relationship between x and $N_{(D \geq 1\ nm)}$ and constancy of $D_{av(\geq 1nm)}$ from one side,[51] and small size, $D_{av(\geq 1nm)}$ ≈ 1.2 nm < 1.5 nm, of the formed nanoparticles from another side.[59]

Figs. 7B – 7D show that the PSDs, established below the CAC at t_s = 3 h (solid curves), do not considerably change during prolonged *rt* aging to $t_s + t_a$ = 24 h (dashed curves). The high stability of the nanoparticles formed below the CAC is caused by at least three reasons: (1) Low concentration of the nanoparticles formed below the CAC substantially reduces the collision frequency between the nanoparticles and thus, reduces the formation of the nanoparticle aggregates. (2) High negative surface charge caused by the formation of deprotonated terminal silanol groups [(NP)Si-OH + OH^- -> (NP)Si-O^- + H_2O] at high concentration, $[OH^-]_{x,t}$, of the unspent OH^- ions at the early stage of TEOS hydrolysis (x << 0.25). (3) Formation of TPA^+ shell around negatively charged nanoparticles[20, 22, 49, 53, 55, 59-61, 63-65] by the attachment of free TPA^+ ions from solution, present in the IM-HmRMs below the CAC. The TPA^+ ions from the shell "block" the terminal silanol groups and thus, prevents the formation of (NP)Si-O-Si(NP) linkages between collided nanoparticles. Hence, it is evident that in this way, the stability of the nanoparticles is caused not only by concentration [1)] and electrostatic [2)][32, 49, 55, 62] reasons, but also by steric ones.[32, 49, 64, 65, 70] Since a part of electrically neutral $Si(OH)_4$ monomers participate in the formation of other oligomers[59, 60, 71] (see also SI-1), it can be assumed that only a small fraction of the $Si(OH)_4$ monomers directly participates in the

formation of the nanoparticles below CAC; this is, by the way, the reason for their low concentration and feasibleness for detection by NMR.

Therefore, atomic force microscopy (AFM) visualization was primarily performed for the identification and presence of nanoparticles that are detected and measured by dynamic light scattering, particularly below the CAC. The AFM cross-section analyzes (middle parts of Fig. 8), along the lines of the corresponding topographic 2D height image of the surface layer of nanoparticles on mica support (left part of Fig. 8) show that the nanoparticles heights lie in the range from about 1 nm to about 2 nm. On the other hand, the lateral half-widths between 35 nm and 50 nm, indicates the association of the individual nanoparticles. Since the nanoparticles have not observed in the "blank" samples (0.25TPAOH:20H_2O - 0.694 M solution of TPAOH; see AFM images and the corresponding section analyzes in Fig. S9 in SI-6), it is evident that AFM height images (right part of Fig. 8) confirm the presence of nanoparticles that have a relative narrow height distribution ranging from 1 to 2 nm. This finding is consistent with the results of other experiments, i.e., that silica nanoparticles, having the average size, $D_{av(\geq 1nm)} \approx 1.2$ nm (see Fig. 7 as well as Fig. S8 and Table S6 in SI-5) form below the CAC.[21,22,24,53] Here must be noted that in all the presented images (Figs. 8 and 10), having the area of 500 nm × 500 nm, the surface-height differentiation, detected by AFM tip is order of magnitude of Å. Since the AFM height and lateral resolution is under 1 nm, and the curvature radius of the sharp AFM probe is below 8 nm, it could be used to characterize the small difference of the surface morphology and the dimensions of aggregates. Thus, the AFM analysis undoubtedly show that a short-time (t_s = 3 h) *rt* stirring of the IM-HmRMs, results in the formation of silica nanoparticles below the CAC (x < 0.25) (Figs. 8Aa and 8Ba,) and that the size of the nanoparticles formed at $t_s \geq 3$ h does not change during prolonged (t_a = 21 h) *rt* aging under static conditions. (Figs. 8Ab and 8Bb). In fact, taking into consideration existence of relatively large fraction of electrically neutral $Si(OH)_4$ monomers below the CAC (10 – 20 % of the $[SiO_2]_{x,tot}$, as was estimated from the data in Table 1 and Fig. 4)

and their role in the formation of silica nanoparticles,[20, 22, 51, 55, 58-61] the formation of silica nanoparticles below the CAC is rather necessity than the rarely expected event.

Analyzes of the data in Fig. 7 and Table S6 in SI-5 show that; (i) the size (1.2 – 1.3 nm) of the nanoparticles formed below the CAC ($x \leq 0.25$) is independent on both x and the time of *rt* stirring/aging, (ii) the size of the nanoparticles formed at t_s = 3 h, increases with increasing value of x, for $x > 0.25$ (above the CAC) and (iii) the nanoparticles present in the IM-HmRMs above the CAC, at $t_s + t_a = 24$ h, are generally smaller than the nanoparticles present in the IM-HmRMs at t_s = 3 h. The above findings lead to an assumption that intensive particulate processes (growth,[51] dissolution,[51] aggregation[53, 72] and disaggregation[56]) simultaneously take place during the *rt* aging of the IM-HmRMs, at least in the time interval from $t_s = t_b$ to $t_s + t_a = 24$ h. To prove (or disapprove) this assumption, the PSD of the particles formed in the IM-HmRMs, having the starting chemical compositions: 1TEOS:0.25TPAOH:20H_2O, was measured at various times t_s (2, 2.5, 3, 3.5 4 and 6 h) and, for a selected sample, at $t_s + t_a = 24$ h.

The DLS-PSD profiles in Figs. 9A – 9C clearly indicate that the size of nanoparticles increases during the *rt* stirring of the IM-HmRM from D_{av} = 4.60 nm at t_s = 2 h (Fig. 9A) through D_{av} = 6.75 nm at t_s = 2.5 h (Fig. 9B) to D_{av} = 7.30 nm at t_s = 3 h (solid curve in Fig. 9C). However, more interesting and important is that the particle size distribution, presented by the solid curve in Fig. 9C, does not represent distribution of the individual (discrete) particles of different sizes (from $D_{min} \approx 2.3$ nm to $D_{max} \approx 22.7$ nm), but rather the aggregates of smaller, individual nanoparticles as can be seen in the AFM height image and its section analysis in Fig. 10. The AFM cross-section analyzes (middle parts of Fig. 10), along the lines of the corresponding topographic 2D height image of the surface layer of nanoparticles on mica support (left parts of Fig. 10), together with the AFM height images (right parts of Fig. 10), show that the individual nanoparticles, protruded above the supported mono-sized particles, have a relative narrow height distribution ranging from 1 to 2 nm (about 1.5 nm in average). On the other hand, since

the lateral half-width is the same (between 10 nm and 15 nm) for the IM-HmRMs stirred for t_s = 3 h (middle part of Fig. 10A) and stirred/aged for $t_s + t_a$ = 24 h (middle part of Fig. 10B), it is evident that the lateral half-widths are related to the lateral dimensions of the aggregates formed during preparation of samples and not to the dimensions of the aggregates formed in the corresponding HmRMs (see Fig. 9C). The large lateral half-widths (between 35 nm and 50 nm) in the cross-section profiles of the individual nanoparticles formed below the CAC (see middle parts of Fig. 8), support this conclusion.

The formation of aggregates of individual (discrete), about 1.5 nm sized (primary) nanoparticles above the CAC (see Figs. 9 and 10) implies that, (a) the nanoparticles are formed by the same mechanism as already is described for the formation of about 1.2 nm sized nanoparticles below the CAC, namely by polymerization via addition of non-pre-associated $Si(OH)_4$ monomers[51, 59] and (b) the nanoparticles, formed as described in (a), are not stabilized either electrostatically[32, 49, 55, 62] or sterically.[32, 49, 64, 65, 70] The implication (a) can be argued by the fact, that a large amount of $Si(OH)_4$ monomers is formed during hydrolysis of TEOS above the CAC, especially for x = 1. This makes the conditions for the formation of increased number (amount) of nanoparticles (see Scheme 1-Ia as well as Figs. S1Aa and S1Ba in SI-1), during the hydrolysis of TEOS above the CAC.[20-22, 24, 25, 27, 28, 35, 44, 45, 49, 51, 53-61] On the other hand, because most of TPAOH is spent for deprotonation of $Si(OH)_4$ monomers [see Eqs. (S2) and (S3) in SI-2)] and formation of TPA-bearing silicate monomers and oligomers (Ogm-TPA species) below the CAC (see SI-2 and SI-7), the concentrations of the free TPA^+ and OH^- ions is low above the CAC[57] (see also Figs. 4, 5bD and Tables 1, S7 and S8). In accordance with the implication (b) this causes that the ≡Si-OH groups are dominant, and the fraction of the ≡Si-O^- groups is considerably reduced on surfaces of the nanoparticles (SiO_2 cores) formed above the CAC[55] (see Scheme 1-Ib); by the same reason, the formed nanoparticles are not sterically stabilized by TPA^+ shell (or this stabilization is very limited) at least to t_s = 3 h (see Schemes 1-I, 1-II and 1-III). Hence, is reasonable to assume that the IM-HmRM (x = 1), obtained by the

complete hydrolysis of TEOS (for $t_s \approx t_b$; see Table 1), above the CAC, is composed of about 1.5 nm sized shell-less silica nanoparticles (SiO_2 cores), dispersed in the water-ethanol solution of TPA-bearing silicate oligomers (mainly 4R, D3R, D4R and D5R; see Figs. 2Aa and 2Ba) and small amount of free TPAOH, at least for $t_b < t_s < 2$ h (see Scheme 1-Ia).

Relatively low ratio Si-Q^3/Si-Q^4 (≈ 1, see Fig. 2Ab) of the nanoparticles indicates that the nanoparticle core is formed mainly by polymerization of $Si(OH)_4$ monomers[51, 55] and that negatively charged silicate monomers and oligomers does not directly participate in the formation of nanoparticle core, as was assumed in some studies.[20, 21, 27, 54, 66] However, still large fraction (about 50 %) of Si with Q^3 sites, is probably caused by a large amount of the surface (terminal) Si atoms, e.g. (core)Si-OH and (core)Si-O^- (see Scheme 1-Ib),[49, 60] but also internal (bulk) ≡Si-OH groups (bordered by red ellipses in Scheme 1-Ic). As already has been mentioned, the ratios Si-Q^3/Si-Q^4 ≈ 1were observed in the silica nanoparticles formed in the concentrated HmRMs.[66, 69, 74] This makes conditions for the formation of (core)Si-O-Si(core) linkages between neighboring, potentially colliding nanoparticle cores (see Scheme 1-II).

Since, above the CAC, most of SiO_2 exist in the form of silica nanoparticles (more than 90 % for x = 1; see Figs. S1Aa and S1Ba in SI-1), intense, high-frequency collisions of the shell-less silica nanoparticles (SiO_2 cores, formed as described above) result in the formation of aggregates (see Scheme 1-IIa) by realization of multiple (core)Si-O-Si(core) linkages between the colliding SiO_2 cores (see Scheme 1-IIb). The size of aggregates gradually increases from $t_s > t_b$ to $t_s = 3$ h (solid curves in Figs. 9A – 9C and Schemes 1-Ia, 1-IIa and 1-IIIa). The formation of aggregates of the shell-less silica nanoparticles was predicted by Rivas-Cardona *et al.*[53]

A wide distribution of sizes of the aggregates, established at $t_s = 3$ h (solid curve in Fig. 9C), indicates that the processes of aggregation (ag in Scheme 1) and disaggregation (d-ag in Scheme 1) are in dynamic equilibrium; however, the forward reaction (ag) is

dominating in the time interval from $t_s > t_b$ to $t_s = 3$ h (see Schemes 1-I – 1-III). On the other hand, since the AFM images and their cross-section analyzes in Fig. 10 show that the nanoparticles present at both $t_s = 3$ h (solid curve in Fig. 9C) and $t_s + t_a = 24$ h (dashed curve in Fig. 9C) represent the aggregates of about 1 nm to 2 nm sized primary nanoparticles, it is evident that the decrease of the particle size from $D_{av} = 7.30$ nm at $t_s = 3$ h to $D_{av} = 3.85$ nm at $t_s + t_a = 3$ h + 21 h = 24 h is caused by a stepwise disaggregation (d-ag) of the aggregates formed in the time interval from $t_s > t_b$ to $t_s = 3$ h. Since the disaggregation, caused by breaking of the (core)Si-O-Si(core) linkages under attack of OH^- ions, cannot be expected at constant or even decreasing alkalinity (see Figs. 4 and 5bD as well as Table S1 in SI-2), only reasonable explanation of the process of disaggregation is blocking of the terminal (core)Si-OH groups and thus, preventing the formation of new (core)Si-O-Si(core) bonds between the colliding nanoparticles, i.e., stoppage of the aggregation. This blocking can be realized by the formation of the shell on the surface of the nanoparticle core. It is reasonable to assume that the shell is firstly formed on the individual silica cores and their small(est) aggregates (see Schemes 1-IIIa and 1-IV); such sterically stabilized entities (SSE) are excluded from the further aggregation processes. Since, as already has been postulated, the aggregation and disaggregation are in dynamic equilibrium (see Schemes 1-Ia, 1-IIa, 1-IIIa and 1-IV), the excluded SSEs are replaced by the disaggregation of the larger aggregates. The disaggregation results in the releasing of individual silica cores and their small(est) aggregates at $t_s \geq 3$ h (see Schemes 1-IIIa, 1-IV and 1-Va). Formation of the shells on the released individual silica cores and their small(est) aggregates, excludes the newly-formed SSEs from the aggregation processes and thus, causes further disaggregation. These processes (exclusion of the SSEs and their replacement by disaggregation) continue until entire amount of the released individual silica cores and their small(est) aggregates has been sterically stabilized by the formation of shells (formation of SSAs at $t_s + t_a \leq 24$ h; see Scheme 1-V) and thus, become unable for aggregation. Such formed SSAs have the

size in the range from $D_{min} \approx 1.6$ nm to $D_{max} \approx 10.9$ nm with $D_p = 3.1$ nm and $D_{av} = 3.85$ nm at $t_s + t_a = 24$ h (see dashed curve in Fig. 9C and Table S6 in SI-5). The AFM image and its cross-section analysis (Fig. 10B) show that the SSAs of different sizes (from about 1.6 nm to about 10.9 nm) are composed of the smaller, about 1 nm to about 2 nm sized primary nanoparticles**.**

Very often, the nanoparticle shell is considered as organic cations (Org^{n+}), usually tetraalkylammonim (TAA^+) and most frequently, TPA^+ ions, adsorbed on the surface of SiO_2 nanoparticle core.[49, 53, 55, 59, 60, 65, 74, 75] This consideration includes association of the Org^{n+} (TAA^+, TPA^+) ions with deprotonated silanol groups[74] and formation of a Stern layer of the adsorbed cations, that is effectively part of the liquid phase of the system.[49, 55] On the other hand, analysis of the interactions of TAA^+ ions with oligomers and nanoparticles (see SI-7) has shown that most of the TPA^+ ions, originally arising from TPAOH, are associated with the polysilicate anions (silicate monomers and oligomers), formed below the CAC.[20-22, 24, 25, 28, 47, 53-57] In addition, from the data presented in Figs. 4 and 5b and Tables 1 and S1, it can be easily calculated that more than 90 % of TPAOH has been spent for deprotonation of the $Si(OH)_4$ monomers, formed during hydrolysis of TEOS, and for the formation of the polysilicate anions (oligomers) associated with TPA^+ ions, below the CAC. Hence, less than 10 % of free (unspent) OH^- ions [$(OH^-)_{x,U,av}$; see Table S7 in SI-7] and consequently, less than 10 % of the free (unspent) TPA^+ ions [$(TPA^+)_{x,U,av}$; see Table S8 in SI-7], are present in the IM-HmRMs above the CAC ($x \geq 0.25$). Finally, knowing that the TPA-silica nanoparticles contains 7 – 15 TPA^+ ions per 100 SiO_2 molecules,[59, 63] it can be easily calculated that $(TPA^+)_{x,U,av} < (TPA^+)_{shell}$ and thus, that amount of the remaining free TPA^+ ions is not sufficient for the formation of the nanoparticle shell (see also SI-7); here, $(TPA^+)_{shell}$ is the fraction (percentage) of the TPA^+ ions needed for the formation of the TPA^+ shell, relative to the starting amount of TPAOH, (see Table S8 in SI-7). Hence, only very small fraction of the TPA^+ ions in the nanoparticle shell is directly bonded to the deprotonated terminal (surface) silanol groups

(see Scheme 1-IIIb). On the other hand, since the majority of the Org^{n+} (TAA^+, TPA^+) ions are associated with the polysilicate anions (oligomers; see SI-7), it is reasonable to conclude that the major part of the nanoparticle shell is formed by the attachment of the polysilicate anions (silicate oligomers), associated with TPA^+ ions, on the surfaces of the nanoparticles cores. This attachment may be realized by the formation of the (core)Si-O-Si(Ogm) linkages between the protonated silanol groups of silica cores [(core)Si-OH] and the protonated silanol groups of silicate oligomers (OgmSi-OH) associated with the Org^{n+} (TAA^+, TPA^+) ions (see Schemes 1-IIIb and 1-Vb).

Since silicate monomers and dimers are precursors for the formation of higher oligomers,[58, 65] it can be assumed that only smaller part of the core surface is covered by the TPA^+-bearing monomers and dimers and thus, that their participation in the formation of the nanoparticle shell is not crucial. However, it is reasonable to assume that these species contribute to Q^1 and Q^2 sites of the nanoparticles (see Figs. 2Ab and 2Bb and Scheme 1-IIIb as well as SI-7), together with the Q^1 and Q^2 sites formed in the bulk of nanoparticle core.[27, 28, 54, 55] Small percentages of the nanoparticles Si atoms having Q^1 and Q^2 sites and their little changes in the time interval from t_s = 3 h (symbols ○ and ● in Figs. 2Ab) to $t_s + t_a$ = 24 h (symbols ○ and ● in Figs. 2Bb) confirm the assumptions that only small amounts of the TPA^+-bearing monomers and dimers participate in the formation of the nanoparticles shells at the early stage of the process (see Scheme 1-IIIb; for the sake of simplicity, only TPA^+-bearing monomers and free TPA^+ ions are displayed as the shell-containing TPA^+ ions). On the other hand, the analysis of the relationships between the types of oligomers attached on the nanoparticle core and their contribution to the distribution of Si-Q sites in the nanoparticles (see SI-7) indicates that the increase of the ratio $Si\text{-}Q^3/Si\text{-}Q^4$ from 0.925 at t_s = 3 h (Fig. 2Ab) to 1.23 at $t_s + t_a$ = 24 h (Fig. 2Bb) is caused by the attachment of the 4DR and 5DR oligomers on the surfaces of the nanoparticles cores. Hence, it can be concluded that the nanoparticle shell is composed of mainly TPA^+-bearing D4R and DR5 oligomers and, as already has been mentioned,

smaller fractions of the TPA^+-bearing monomers and dimers, at $t_s + t_a = 24$ h (see Scheme 1-Vb; for the sake of simplicity, only the simplified, "2D sketchs" of the TPA^+-bearing D4R and D5R units are presented in the scheme). Assuming that the mobility of the Ogm-TPA species are considerably lower than the mobility of the TPA^+ ions and that the mobility decreases with the increasing size of the Ogm-TPA species, the formation of the nanoparticle shell by the attachment of the larger oligomers (D4R and D5R), explains the "delaying" in the formation of the shell: It is reasonable to assume that the first Ogm-TPA species attached on the nanoparticle core are $Si(OH)_3O^{-\cdots+}TPA$ (monomers) and/or $(OH)_3Si\text{-}O\text{-}Si(OH)_2O^{-\cdots+}TPA$, $TPA^{+\cdots-}O(OH)_2Si\text{-}O\text{-}Si(OH)_2O^{-\cdots+}TPA$ (dimers) (see Scheme 1-IIIb). By the same principles, larger Ogm-TPA species, (D4R and D5R) attach to the surfaces of the nanoparticles cores later ($t_s > 3$ h).

Finally, it is reasonable to assume that the TPA^+ ions overlay not only directly interacting silanol groups of the attached oligomers, but also surrounding ones, (see Scheme 1-Vb). In this way, the terminal silanol groups of the TPA-containing oligomers (shell) are unable for the formation of (new) (NP)Si-O-Si(NP) linkages between eventually collided core@shell nanoparticles (NP). As already has been pointed out, this is the reason that the steric stabilization of the nanoparticles, caused by the formation of shells, as described above, not only prevents the further aggregation, but also provokes disaggregation of the already formed aggregates (see Fig. 9 and Scheme 1), which results in the establishing of the stable particulate system composed of small aggregates of primary silica nanoparticles (dashed curve in Fig. 9C, AFM image in Fig. 10B and Scheme 1-V.

CONCLUSIONS

The clear solutions in the system, SiO_2-TPAOH-EtOH-H_2O, prepared by room-temperature (*rt*) hydrolysis of TEOS (tetraethyl orthosilicate) in the reaction mixtures having the starting chemical compositions: xTEOS:0.25TPAOH:20H_2O, were

characterized by different methods during the preparation (measuring of pH and ionic conductivity) and during subsequent *rt* stirring/aging (^{29}Si-NMR, DLS, AFM).

Careful analysis of the obtained data clearly shows that the results of this study offer some new elements for the understanding of the mechanisms of formation and room temperature evolution of the core@shell silica nanoparticles:

(1) In spite of widely spread meaning that the silica nanoparticle cannot be formed below the critical aggregation concentration (CAC; $x < 0.25$) of SiO_2, the resolute evidence of the formation of the stable, about 1.2 nm sized core(amorphous SiO_2)@shell(TPA^+ ions) nanoparticles below the CAC was found during realization of this study. The nanoparticle core, formed by polymerization via addition of the $Si(OH)_4$ monomers which are not pre-associated with OSDA (organic structure-directing agents - TPA^+ in the studied case), are immediately stabilized electrostatically (deprotonation of the surface silanol groups at high $[OH^-]/[SiO_2]$ ratio below the CAC) and sterically (formation of the TPA^+ shell on the surface of the nanoparticle core at high $[TPA^+]/[SiO_2]$ ratio below the CAC). Due to the small fraction of the SiO_2 in the form of nanoparticles below the CAC, they cannot be evidenced by ^{29}Si-MNR, but can be clearly detected by DLS and observed by AFM.

(2) The nanoparticles formed above the CAC, aggregate into larger particles in the short time interval from $t_s < 2$ h to $t_s \leq 3$ h; the larger particles are composed of discrete (individual) 1 – 2 nm sized primary nanoparticles formed at $t_s < 2$ h. This indicates that due to insufficient concentration of TPAOH, the nanoparticles formed above the CAC are not stabilized either electrostatically or sterically, at least to $t_s \approx 3$ h. Of course, the indicated time intervals are valid for the investigated IM-HmRMs having the starting chemical compositions: $TEOS:0.25TPAOH:20H_2O$; it can be expected that the characteristic time intervals changes with the change of the (starting) chemical composition of HmRMs.

(3) Disaggregation of the particles (aggregates), formed above the CAC, in the time interval from $t_s < 2$ h to $t_s \leq 3$ h, as described in (2), start to disaggregate at 3 h $\leq t_s \leq$ 3.5 h as the consequence of the stepwise formation of the shell on the surface of the nanoparticle core (steric stabilization) and thus, by exclusion of the stabilized nanoparticles (SSAs) from further aggregation processes. Since the processes of aggregation and disaggregation are in dynamic equilibrium, the excluded nanoparticles and their small aggregates are replaced by the disaggregation of larger aggregates. These processes (exclusion of the stabilized nanoparticles and their replacement by disaggregation) continue until entire amount of nanoparticles and their small aggregates has been sterically stabilized by the formation of shells (at $t_s + t_a \leq 24$ h) and thus, unable for aggregations. In this way, the stabilized core@shell nanoparticles are not individual (discrete) entities, but the nanoaggregates of the primary nanoparticles.

(4) On the basis of the estimated ratio $[TPA^+]/[SiO_2]$ ([shell]/[core]) in the core@shell silica nanoparticles and the known concentrations of the remaining (free) TPAOH above the CAC, it is concluded that the nanoparticle shell can be formed only by attachment of the polysilicate anions (silicate oligomers), associated with TPA^+ ions, on the surfaces of the nanoparticles cores. This gives a new insight in the "structure" of the nanoparticle shell, which is considerably different from the most frequently described one, i.e., free TPA^+ ions adsorbed on the surface of the nanoparticle core.

Since the general mechanism of the formation of the core(amorphous silica)@shell(Org^{n+} ions) nanoparticles does not depend on the nature of organic cation (Org^{n+}) and the ratios $[TEOS]/[Org(OH)_n]$ and $[TEOS]/[H_2O]$,[28, 56] it is reasonable to conclude that the results obtained in this work are imminent not only for the investigated reaction mixtures, but also for other reaction mixtures in the systems, TEOS-$Org(OH)_n$-H_2O and thus, have the general significance.

ASSOCIATED CONTENT

Supporting Information

The Supporting Information is available free of charge on the ACS Publications website. Additional analyzes of ^{29}Si-NMR data; measurement and correction of pH values with respect to ethanol content; simulation (calculation) of the changes in the relevant concentrations during room-temperature stirring (aging) of the investigated homogeneous reaction mixtures; analysis of the changes in the concentrations, [SiO_2], of silica and, [OH^-], of OH^- ions and of their relationships at various stages of hydrolysis of TEOS in the investigated homogeneous reaction mixtures; analysis of the DLS-PSD data; AFM images of the "blank" sample; analysis of interactions of tetraalkylammonium (TAA+) ions with silica oligomers and nanoparticles;additional references (PDF)

AUTHOR INFORMATION

Corresponding Author
*boris.subotic@irb.hr
ORCID
Boris Subotic: 0000-0002-3589-7845

Notes

The authors declare no competing financial interest.

ACKNOWLEDGMENTS

This work is supported by Croation Science Fundation, under project IP-2016-06-2214 and IP-2016-06-8415. Author VS received funding for equipment from the Ministry of Science and Education of the Republic of Croatia.

REFERENCES

(1) Corma, A. Inorganic Solid Acids and Their Use in Acid-Catalyzed Hydrocarbon Reactions. *Chem. Rev.* **1995**, *95*, 559-614.
(2) Davis, M. E. Ordered Porous Materials for Emerging Applications. *Nature* **2002**, *417*, 813-821.
(3) Yu, J.; Xu, R. Insight into Construction of Open-Framework Aluminophosphates. *Chem. Soc. Rev*. **2006**, *35,* 593-604.

(4) Zaarour, M.; Dong. B.; Naydenova, I.; Retoux, R.; Mintova, S. Progress in Zeolite Synthesis Promotes Advanced Applications. *Microporous Mesoporous Mater*. **2014**, *189*, 11-21.

(5) Subotić, B.; Bronić, J.; Antonić Jelić, T. Theoretical and Practical Aspects of Zeolite Nucleation. In *Ordered porous solids*, Valtchev, V.; Mintova, S.; Tsapatsis, M., Eds. Elsevier: Amsterdam, The Netherlands, 2008; pp 127−185.

(6) Lok, B. M.; Cannan, T. R.; Messina, C. A. The Role of Organic Molecules in Molecular Sieve Synthesis: Review Article. *Zeolites*, **1983**, *3*, 282-291.

(7) Breck, D. W.; Eversole, W. G.; Milton, R. M. New Synthetic Crystalline Zeolites. *J. Am. Chem. Soc*. **1956**, *78*, 2338-2339.

(8) Zhdanow, S. P. Some Problems in Zeolite Crystallization. *Adv. Chem. Ser*. **1971**, *101*, 20-43.

(9) Breck, D. W. *Zeolite molecular sieves*; Wiley: New York, N.Y., 1974.

(10) Subotić, B.; Bronić, J. Theoretical and Practical Aspects of Zeolite Crystal Growth. In *Handbook of Zeolite Science and Technology*, Auerbach, S. M.; Carrado, K. A.; Dutta, P. K., Eds. Marcel Dekker Inc.: New York – Basel, 2003; pp 129-203.

(11) Barrer, R. M. *Hydrothermal Chemistry of Zeolites*; Academic Press: London, U.K., 1982.

(12) Cundy, C.S.; Cox, P. A. The Hydrothermal Synthesis of Zeolites: History and Development from the Earliest Days to the Present Time. *Chem. Rev*. **2003**, *103*, 633-701.

(13) Cundy, C. S.; Cox, P. A. The Hydrothermal Synthesis of Zeolites: Precursors, Intermediates and Reaction Mechanisms: Review Article. *Microporous Mesoporous Mater*. **2005**, *82*, 1-78.

(14) Sameen, S.; Zaidi, A.; Rohani, S. Progress Towards a Dry Process for the Synthesis of Zeolite – A Review. *Rev. Chem. Eng*. **2005**, *21***,** 265-306.

(15) Mintova, S.; Gilson, J.-P.; Valtchev, V. Advances in Nanosized Zeolites. *Nanoscale* **2013**, *5*, 6693-6703.

(16) Maldonado, M.; Oleksiak, M. D.; Chinta, S.; Rimer, J. D. Controlling Crystal Polymorphism in Organic-Free Synthesis of Na-Zeolites. *J. Am. Chem. Soc*. **2013**, *135*, 2641-2652.

(17) Oleksiak, M. D.; Rimer, J. D. Synthesis of Zeolites in the Absence of Organic Structure-Directing Agents: Factors Governing Crystal Selection and Polymorphism. *Rew. Chem. Eng*. **2014**, *30*, 1-49.

(18) de Moor, P.-P. A.; Beelen, T. P. M.; Komanschek, B. U.; Diat, O.; van Santen, R. A. In Situ Investigation of Si-TPA-MFI Crystallization Using (Ultra-) Small- and Wide-Angle X-Ray Scattering. *J. Phys. Chem. B* **1997**, *101*, 11077-11086.

(19) de Moor, P.-P. A.; Beelen, T. P. M.; Komanschek, B. U.; Beck, L. W.; Wagner, P.; Davis, M. E.; van Santen, R. A. Imaging the Assembly Process of the Organic-Mediated Synthesis of a Zeolite. *Chem. Eur. J.* **1999**, *5*, 2083-2088.

(20) Fedeyko, J. M.; Rimer, J. D.; Lobo, R. F.; Vlachos, D. G. Spontaneous Formation of Silica Nanoparticles in Basic Solutions of Small Tetraalkylammonium Cations. *J. Phys. Chem. B* **2004**, *108*, 12271-12275.

(21) Yang, S.; Navrotsky, A. Early-Stage Reactions in Synthesis of TPA-Silicalite-1: Studies by in Situ Calorimetry, SAXS and pH Mesurements. *Chem. Mater*. **2004**, *16*, 3682-3687.

(22) Fedeyko, J. M.; Vlachos, D. G.; Lobo, R. F. Formation and Structure of Self-Assembled Silica Nanoparticles in Basic Solutions of Organic and Inorganic Cations. *Langmuir* **2005**, *21*, 5197-5206.

(23) Cheng, C.-H.; Shantz, D. F. Nanoparticle Formation and Zeolite Growth in TEOS/Organocation/Water Solutions. *J. Phys. Chem. B*. **2005**, *109*, 7266-7274.

(24) Castro, M.; Haouas, M.; Taulelle, F.; Lim, I.; Breynaert, E.; Brabants, G.; Kirschhock, C. E. A.; Schmidt, W. Multidiagnostic Analysis of Silicate Speciation in Clear Solutions/Sols for Zeolite Synthesis. *Microporous Mesoporous Mater*. **2014**, *189*, 158-162.

(25) Fedeyko, J. M.; Eglof-Fox, H.; Fickel, D. W.; Vlachos, D. G.; Lobo, R. F. Initial Stages of Self-Organization of Silica-Alumina Gels in Zeolite Synthesis. *Langmuir* **2007**, *23*, 4532-4540.

(26) Wu, Y.- S.; Chiang, A. S. T.; Tsai, T.-C. Some Observations on the Synthesis of Colloidal Beta Zeolite from a Clear Precursor Sol. *Sci. Adv. Mater*. **2011**, *3*, 1011-1018.

(27) Hould, N. D.; Haouas, M.; Nikolakis, V.; Taulelle, F.; Lobo. R. Mechanisms of Quick Zeolite Beta Crystallization. *Chem. Mater.* **2012**, *24,* 3621-3632.

(28) Eilertsen, E. A.; Haouas, M.; Pinar, A. B.; Hould, N. D.; Lobo, R. F.; Lillerud, K. P. Taulelle, F. NMR and SAXs Analysis of Connectivity of Aluminium and Silicon Atoms in Clear Sol Precursors of SSZ-13 Zeolite. *Chem. Mater*. **2012**, *24*, 571-578.

(29) Schoeman, B. J.; Sterte, J.; Otterstedt, J.-E. Colloidal Zeolite Suspensions. *Zeolites* **1994**, *14*, 110-116.

(30) Schoeman, B. J. A High Temperature in Situ Laser Light-Scattering Study of the Initial Stage in the Crystallization of TPA-Silicalite-1. *Zeolites* **1997**, *18*, 97-105.

(31) Mintova, S.; Petkov, N.; Karaghiosoff, K.; Bein, T. Transformation of Amorphous Silica Colloids to Nannosized MEL Zeolite. *Microporous Mesoporous Mater*. **2001**, *50*, 121-128.

(32) Yang, S.; Navrotsky, A.; Wesolowski, D. J.; Pople, J. A. Study on the Synthesis of TPA-Silicalite-1 from Initially Clear Solutions of Various Base Concentrations by in Situ Calorimetry, Potentiometry, and SAXS. *Chem. Mater.* **2004**, *16*, 210-219.

(33) Cheng, C.-H.; Shantz, D. F. Small-Angle Scattering Studies of Silicalite-1 Growth from Clear Solutions. *Curr. Opin*. *Colloid Interface Sci*. **2005**, *10*, 188-194.

(34) Larlus, O.; Mintova, S.; Bein, T. Environmental Synthesis of Nanosized Zeolites with High Yield and Monomodal Particles Size Distribution. *Microporous Mesoporous Mater*. **2006**, *96*, 405-412.

(35) Aerts, A.; Haouas, M.; Caremans, T. P.; Follens, L. R. A.; van Erp, T. S.; Taulelle, F.; Martens, J. A.; Kirschhock, C. E. A. Investigation of the Mechanism of Colloidal Silicalite-1 Crystallization by Using DLS, SAXS, and ^{29}Si NMR Spectroscopy. *Chem. Eur. J.* **2010**, *16*, 2764-2774.

(36) Ng, E.-P.; Chateigner, D.; Bein, T.; Valtchev, V.; Mintova, S., Capturing Ultrasmall EMT Zeolite from Template-Free Systems. *Science*, **2012**, *335*, 70-73.

(37) Kosanović, C.; Havenscak, K.; Subotić, B.; Svetličić, V.; Mišić, T.; Cziraki, A.; Huhn, G. A Contribution to Understanding the Mechanism of Crystallization of Silicalite-1 in Heterogeneous Systems (Hydrogels). *Microporous and Mesoporous Materials* **2009**, *123*, 150-159.

(38) Ren, N.; Bosnar, S.; Bronić, J.; Dutour Sikirić, M.; Mišić, T.; Svetličić, V.; Mao, J.-J.; Antonić Jelić, T.; Hadžija, M.; Subotić, B. Role of Subcolloidal (Nanosized) Precursor Species in the Early Stage of Crystallization of Zeolites in Heterogeneous Systems. *Langmuir* **2014**, *30*, 8570-8579.

(39) Burkett, S. L.; Davis, M. E. Mechanism of Structure Direction in the Synthesis of Si-ZSM-5: An Investigation by Intermolecular ^{1}H-^{29}Si CP MAS NMR. J. *Phys. Chem*. **1994**, *98*, 4647-4653.

(40) Burkett, S. L.; Davis. M. E. Mechanism of Structure Direction in the Synthesis of Pure Silica Zeolites. *Chem. Mater*. **1995**, *7*, 920-928.

(41) Regev, O.; Cohen, Y.; Kehat, E.; Talmon, Y. Precursors to the Zeolite ZSM-5 Imaged by Cryo-TEM and Analyzed by SAXS. *Zeolites* **1994**, *14*, 314-319.

(42) Dokter, W. H.; van Garderen, H. F.; Beelen, T. P. M.: van Santen, R. A.; Bras, V. Homogeneous Versus Heterogeneous Zeolite Nucleation. *Angew. Chem. Int. Ed. Engl.* **1995**, *34*, 73-75.

(43) Iler, R. K. *The Chemistry of Silica: Solubility, Polymerization, Colloid and Surface Properties and Biochemistry*; Wiley: New York, N.Y., 1979.

(44) Kinrade, S. D.; Knight, C. T. G.; Pole, D. L.; Syvitski, R. T. Silicon-29 NMR Studies of Tetraalkylammonim Silicate Solutions. 1. Equilibria, (29)Si Chemical Shifts, and (29)Si Relaxation. *Inorg. Chem*. **1998**, *37,* 4272-4277.

(45) Kinrade, S. D.; Del Nin, J. W.; Schach, A. S.; Sloan, T. A.; Wilson, K. L.; Knight, C. T. G. Stable Five- and Six-Coordinated Silicate Anions in Aqueous Solution. *Science* **1999**, *285*, 1542-1545.

(46) Kinrade, S. D.; Donovan, J. C. H.; Schach, A. S.; Knight, C. T. G. Two Substituted Cubic, Octameric Silicate Cages in Aqueous Solutions. *J. Chem. Soc. Dalton Trans.* **2002**, 1250-1252.

(47) Rimer, J. D.; Vlachos, G. D.; Lobo, R. F. Evolution of Self-Assembled Silica-Tetrapropylammonium Nanoparticles at Elevated Temperatures. *J. Phys. Chem. B* **2005**, *109*, 12762-12771.

(48) Cheng, C.-H.; Shantz, D. F. Silicalite-1 Growth from Clear Solution: Effect of Alcohol Identity and Content on Growth Kinetics. *J. Phys. Chem. B* **2005**, *109*, 19116-19125.

(49) Rimer, J. D.; Lobo, R. F.; Vlachos. D. G. Physical Basis of the Formation and Stability of Silica Nanoparticles in Basic Solutions of Monovalent Cations. *Langmuir* **2005**, *21*, 8960-8971.

(50) Cheng, C.-H.; Shantz, D. F. Silicalite-1 Growth from Clear Solution: Effect of Structure Directing Agent on Growth Kinetics. *J. Phys. Chem. B* **2005**, *109*, 13912-13920.

(51) Provis, J. L.; Vlachos, D. G. Silica Nanoparticle Formation in the TPAOH-TEOS-H_2O System: A Population Balance Model. *J. Phys. Chem. B* **2006**, *110*, 3098-3108.

(52) Follens, L. R. A.; Aerts, A.; Haouas, M.; Caremans, T. P.; Loppinet, B.; Goderis, B.; Vermant, J.; Taulelle, F.; Martens, J. A.; Kirschhock, C. E. A. Characterization of Nanoparticles in Diluted Clear Solutions for Silicalite-1 Zeolite Synthesis Using Liquid ^{29}Si NMR, SAXS and DLS. *Phys. Chem. Chem. Phys*. **2008**, *10*, 5574-5583.

(53) Rivas-Cardona, A.; Chovanetz, M.; Shantz, D. F. A Systematic Investigation of Silicalite-1 Precursor Mixtures with Varying Degrees of Dilution. *Microporous Mesoporous Mater*. **2012**, *155*, 56-64.

(54) Petry, D. P.; Haouas, M.; Wong, S. C. C.; Aerts, A.; Kirschhock, C. E. A.; Martens, J. A.; Gaskell, S. J.; Anderson, M. W.; Taulelle, F. Connectivity Analysis of the Clear Sol Precursor of Silicalite: Are Nanoparticles Aggregated Oligomers or Silica Particles? *J. Phys. Chem. C*, **2009**, *113*, 20827-20836.

(55) Rimer, J. D.; Fedeyko, J. M.; Vlachos, D. G., Lobo, R. F. Silica Self-Assembly and Synthesis of Microporous and Mesoporous Silicates. *Chem. Eur. J.* **2006**, *12*, 2926-2934.

(56) Caremans, T. P.; Loppinet, B.; Follens, L. R. A.; van Erp, T. S.; Vermant, J.; Goderis, B.; Kirschhock, C. E. A.; Martens, J. A.; Aerts, A. Invesigation of Nanoparticles Occurring in the Colloidal Silicalite-1 Zeolite Crystallization Process Using Dissolution Experiments. *Chem. Mater*. **2010**, *22*, 3619-3629.

(57) Castro, M.; Haouas, M.; Lim, I.; Bongard, H. J.; Schüth, F.; Taulelle, F.; Karlsson, G.; Alfredsson, V.; Breyneart, E.; Kirschhock, C. E.; Schmidt, W. Zeolite Beta Formation from Clear Sols: Silicate Speciation, Particle Formation and Crystallization Monitored by Complementary Analysis Methods. *Chem. Eur. J.* **2016**, *22*, 15307-15319.

(58) Matsoukas, T.; Gulari, E. Monomer-Addition Growth With Slow Initiation Step: A Growth Model for Silica Particles from Alkoxides. *J. Coll. Interf. Sci.* **1989**, *132*, 13-21.

(59) Chien, S. C.; Auerbach, S. M.; Monson, P. A. Modeling of the Self-Assembly of Silica-Templated Nanoparticles in the Initial Stages of Zeolite Formation. *Langmuir* **2015**, *31*, 4940-4949.

(60) Jorge, M.; Auerbach, S. M.; Monson, P. A. Modelling of Spontaneous Formation of Precursor Nanoparticles in Clear-Solution Zeolite Synthesis. *J. Am. Chem. Soc*. **2005**, *127*, 14388-14400.

(61) Auerbach, S. M.; Ford, M. H.; Monson, P. A. New Insights into Zeolite Formation from Molecular Modeling. *Curr. Opin. Colloid Interface Sci.* **2005**, *10*, 220 – 225.

(62) Nikolakis, V.; Kokkoli, E.; Tirrell, M.; Tsapatsis, M.; Vlachos, D. G. Zeolite Growth by Addition of Subcolloidal Particles: Modeling and Experimental Validation. *Chem. Mater*. **2000**, *12*, 845-853.

(63) Rivas-Cardona, A.; Shantz, D. F. Pulsed Field Gradient Investigations of Alkytripropylammonium-Silica Mixtures. *J. Phys. Chem. C* **2010**, *114*, 20178-20188.

(64) Hould, N. D.; Foster, A.; Lobo, R. F. Zeolite Beta Mechanism of Nucleation and Growth. *Microporous Mesoporous Mater*. **2011**, *142*, 104-115.

(65) Davis, T. M.; Drews, T. O.; Ramanan, H.; He, C.; Dong, J.; Schnablegger, H.; Katsoulakis, M. A.; Kokkoli, E.; McCormick, A. V.; Lee Penn, R.; Tsapatsis, M. Mechanistic Principles of Nanoparticle Evolution to Zeolite Crystals. *Nature Mater*. **2006**, *5*, 400-408.

(66) Haouas, M.; Petry, D. P.; Anderson, M. W.; Taulelle, F. ^{29}Si NMR Relaxation of Silicated Nanoparticles in Tetraethoxylane-Tetrapropylammonium Hydroxide-Water System (TEOS-TPAOH-H_2O). *J. Phys. Chem. C* **2009**, *113*, 10838-10841.

(67) Rao N. D.; Gelb, L. D. Molecular Dynamics Simulations of the Polymerization of Aqueous Silicic Acid and Analysis of the Effects of Concentration on Silica Polymorph Distributions, Growth Mechanisms, and Reaction Kinetics. J. *Phys. Chem. B* **2004**, *108*, 12418– 12428.

(68) Massiot, D.; Fayon F.; Capron M.; King I.; Le Calvé S.; Alonso B.; Durand J. O.; Bujoli, B.; Gan Z.; Hoatson, G. Modelling One- and Two-Dimensional Solid-State NMR Spectra. *Magn. Reson. Chem.* **2002**, *40*, 70-76.

(69) Kragten, D. D.; Fedeyko, J. M.; Sawant, K. R.; Rimer, J. D.; Vlachos, D. G.; Lobo, R. F.; Tsapatsis, M. Structure of the Silica Phase Extracted from Silica/(TPA)OH Solutions Containing Nanoparticles. *J. Phys. Chem. B* **2003**, *107*, 10006–10016.

(70) Schoeman, B. J. Analysis of the Nucleation and Crystal Growth of TPA-Silicalite-1 at Elevated Temperatures with the Emphasis on Colloidal Stability. *Microporous Mesoporous Mater*. **1998**, *22*, 9-22.

(71) Mora-Fonz, M. J.; Catlow, C. R. A.; Lewis, D. W. Oligomerization and Cyclization Processes in the Nucleation of Microporous Silicas. *Angew. Chem. Int. Ed*. **2005**, *44*, 3082-3086.

(72) van Tendeloo, L.; Haouas, M.; Martens, J. A.; Kirschhock, C. E. A.; Breynaert, E.; Taulelle, F. Zeolite Synthesis in Hydrated Silicate Ionic Liquids. *Faraday Discuss*. **2015**, *179*, 437−449.

(73) Ravishankar, R.; Kirschhock, C. E. A.; Knops-Gerrits, P.; Feijen, E. J. P.; Grobet, P. J.; Vanoppen, P.; de Schryver, F. C.; Miehe, G.; Fuess, H.; Schoeman, B. J.; et al. Characterization of Nanosized Material Extracted from Clear Suspensions of MFI Zeolite Systems. *J. Phys. Chem. B* **1999**, *103*, 4960-4964.

(74) Nikolakis, V.; Tsapatsis, M.; Vlachos, D. G. Physicochemical Characterization of Slicalite-1 Surface and Its Implications on Crystal Growth. *Langmuir* **2003**, *19*, 4619–4626.

(75) Hould, N. D.; Lobo, R. F. Nanoparticle Precursors and Phase Selectivity in Hydrothermal Synthesis of Zeolite Beta. *Chem. Mater.* **2008,** *20,* 5807–5815.

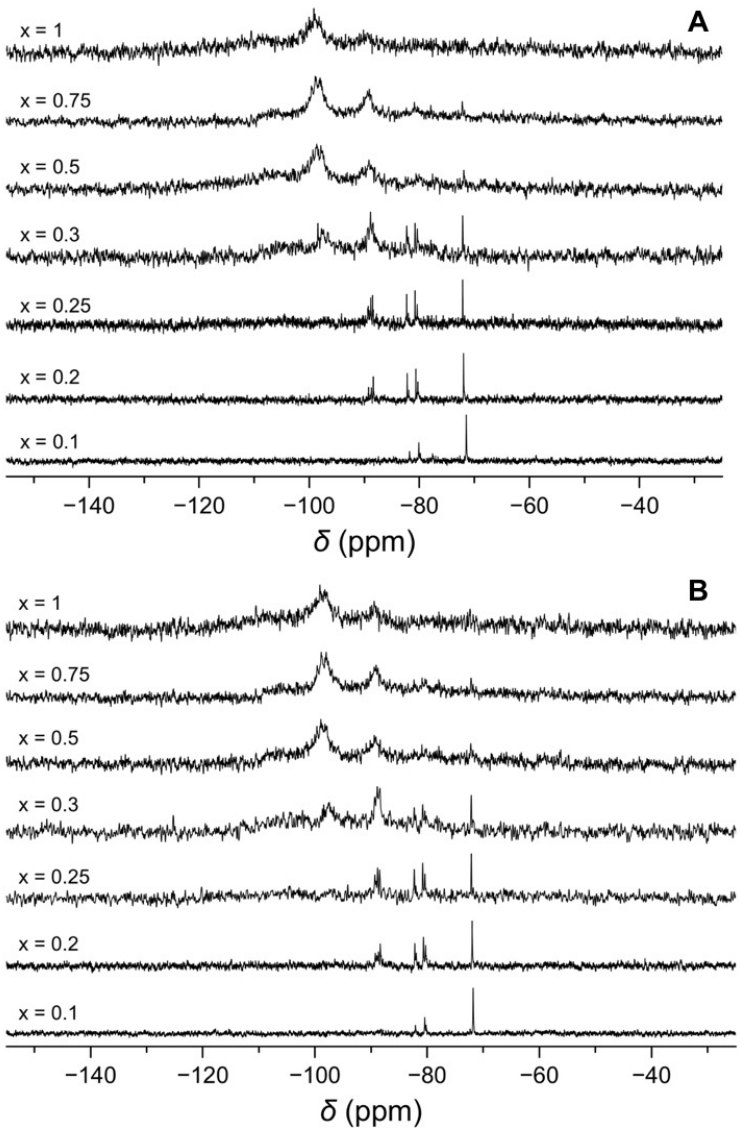

Figure 1 ^{29}Si-NMR spectra of the homogeneous reaction mixtures (clear solution) obtained by room-temperature (*rt*) stirring for t_s = 3 h (A) and then by additional room-temperature aging, under static conditions, for t_a = 21 h (B), of the investigated "model" homogeneous reaction mixtures (IM-HmRMs) having the initial molar compositions: xTEOS:0.25TPAOH:20H_2O (see Experimental methods).

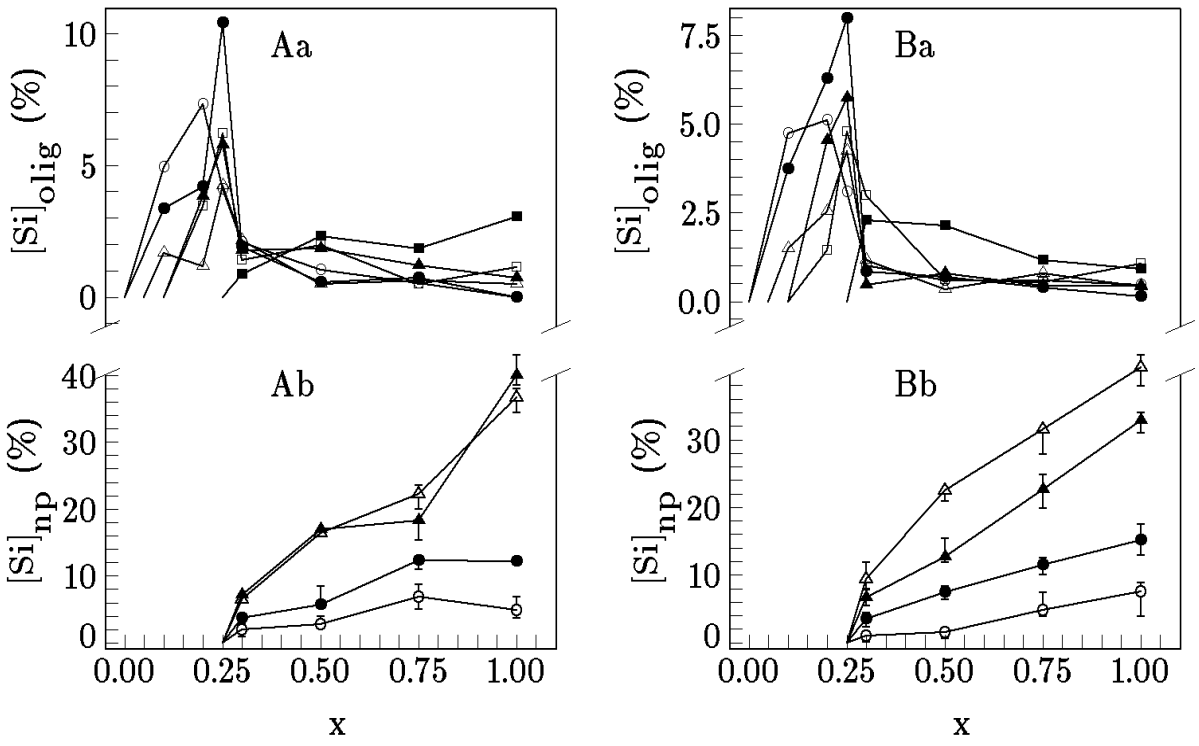

Figure 2 Si-distribution in oligomers (Aa, Ba) and distribution of Q^n Si atoms (Q^n sites) in nanoparticles (Ab, Bb), as functions of x, in the homogeneous reaction mixtures (clear solution) obtained by room-temperature (*rt*) stirring for t_s = 3 h (Aa, Ab) and then by additional *rt* aging, under static conditions, for t_a = 21 h (Ba, Bb) of the IM-HmRMs. The corresponding symbols in Figs. Aa and Ba are: ○ for monomers, ● for dimers, △ for cyclic trimers (3R), ▲ for cyclic tetramers (4R), □ for double three rings (D3R), ■ for double four rings (D4R) and double five rings (D5R). The corresponding symbol in Figs Ab and Bb are: ○ for mixture of Q^1 and $Q^{2\Delta}$ sites, ● for mixture of Q^2 and $Q^{3\Delta}$ sites, △ for Q^3 sites and ▲ for Q^4 sites. Here $Q^{n\Delta}$ corresponds to Si sites with n connectivity present in 3-membered rings. The errors of the values of $[Si]_{olig}$ (Aa and Ba) vary from ±0.1 % to ±0.5 % and are independent on x.

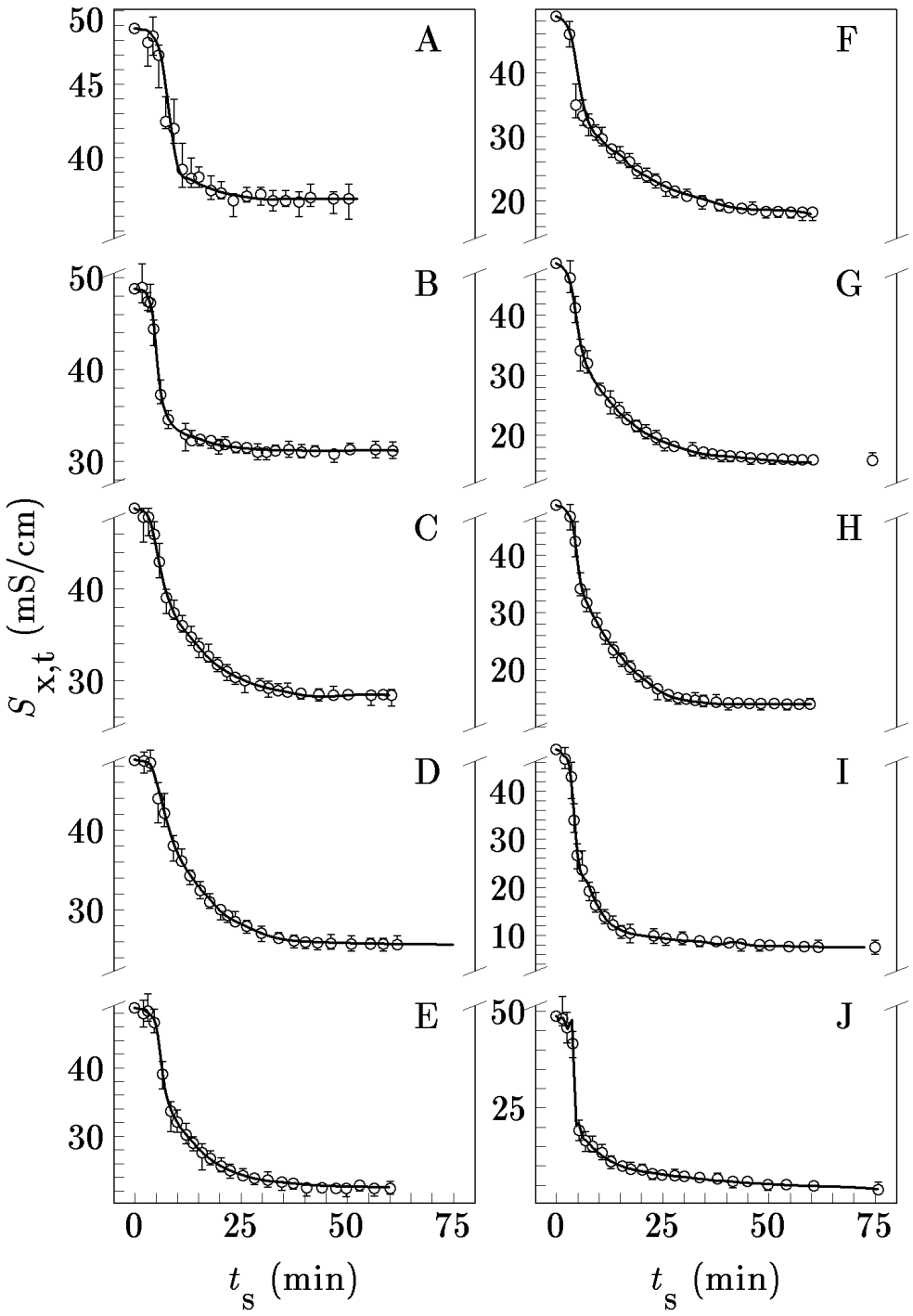

Figure 3 Changes of the ionic conductivity, $S_{x,t}$, measured during preparation and aging of the IM-HmRMs with with x = 0.05 (A), 0.1 (B), 0.125 (C), 0.15 (D), 0.175 (E), 0.2 (F), 0.22 (G), 0.25 (H), 0.5 (I) and 1.0 (J). The IM-HmRMs were prepared by the *rt* stirring of the reaction mixtures having the starting chemical compositions: xTEOS:0.25TPAOH:20H_2O. t_s is the time of aging (with stirring) passed from the mixing of TEOS and TPAOH solutions (see Experimental methods).

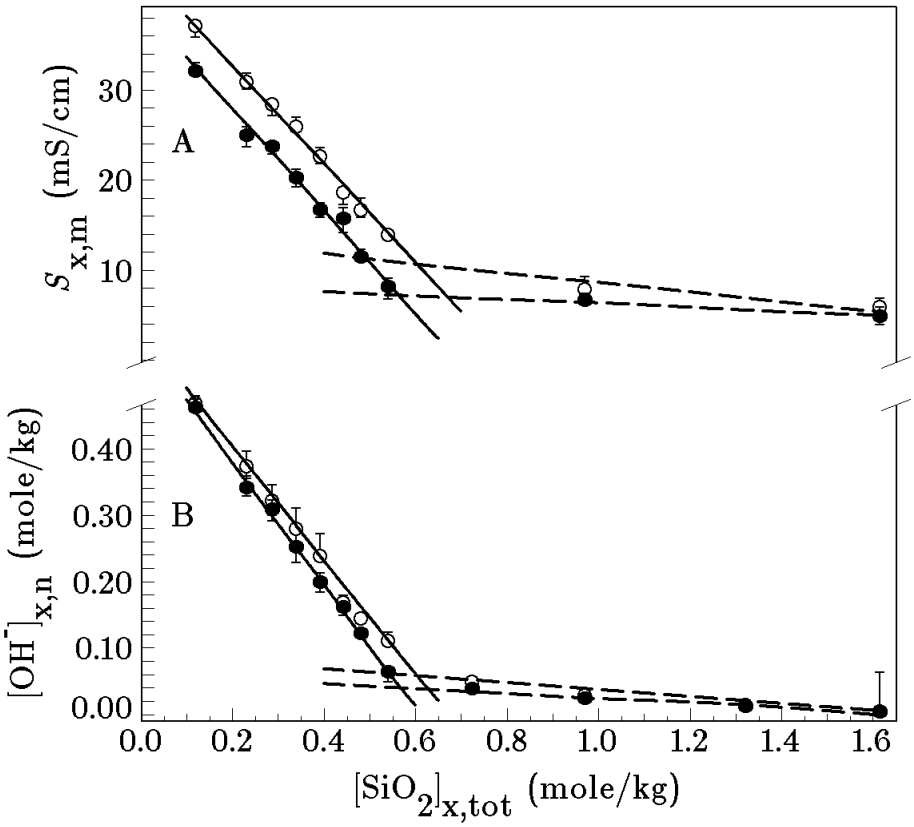

Figure 4 Changes of (A) the ionic conductivity, $S_{x,m}$, measured at "equilibrium" time $t_s = t_{eq}$ (○; m = eq; see Table 1) and at $t_s + t_a = 24$ h (●, m = 24h) and (B) the concentrations, $[OH]_{x,n}$, of the OH^- ions measured at the "breakthrough" time $t_s = t_b$ (○; n = b) and at $t_b + t_a = 24$ h (●, n = 24h), with the concentration, $[SiO_2]_{x,tot}$, of the SiO_2 formed by hydrolysis of TEOS in the IM-HmRMs. The corresponding values of t_{eq} and t_b are listed in Table 1.

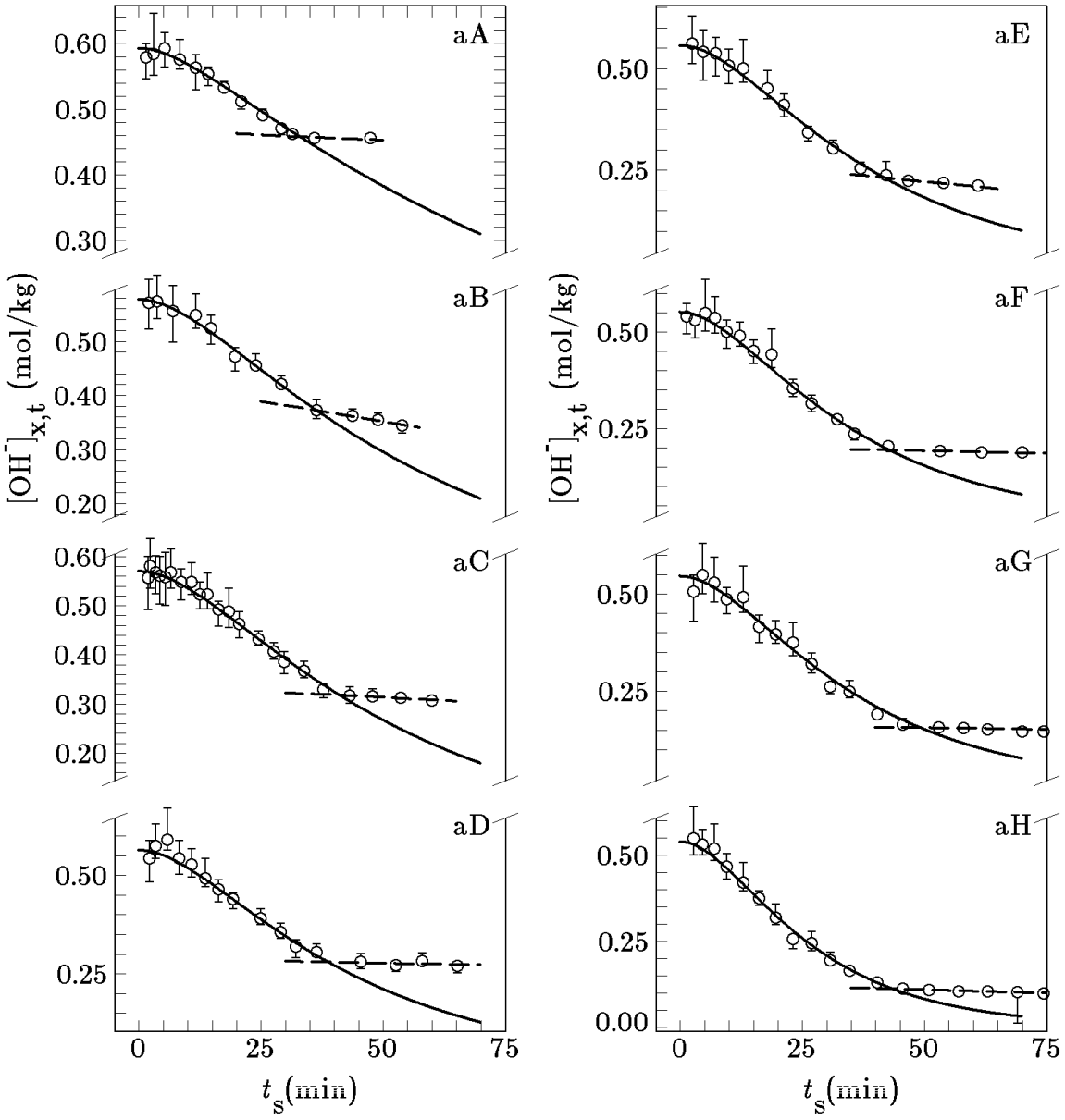

Figure 5a Changes in the molality concentrations, $[OH^-]_{x,t}$ of the OH^- ions during preparation and aging of the IM-HmRMs with with x = 0.05 (aA), 0.1 (aB), 0.125 (aC), 0.15 (aD), 0.175 (aE), 0.2 (aF), 0.22 (aG) and 0.25 (aH). The IM-HmRMs were prepared by the *rt* stirring of the reaction mixtures having the starting chemical compositions: xTEOS:0.25TPAOH:20H_2O. The values of $[OH^-]_{x,t}$, characterized by symbol ○, are determined (calculated) from the corresponding measured and corrected pH values (see SI-2) and the values of $[OH^-]_{x,t}$, characterized by solid curves, are calculated by simultaneous numerical solutions of the equations (1) and (2). t_s is the time of aging (with stirring), passed from the mixing of TEOS and TPAOH solutions (see Experimental methods).

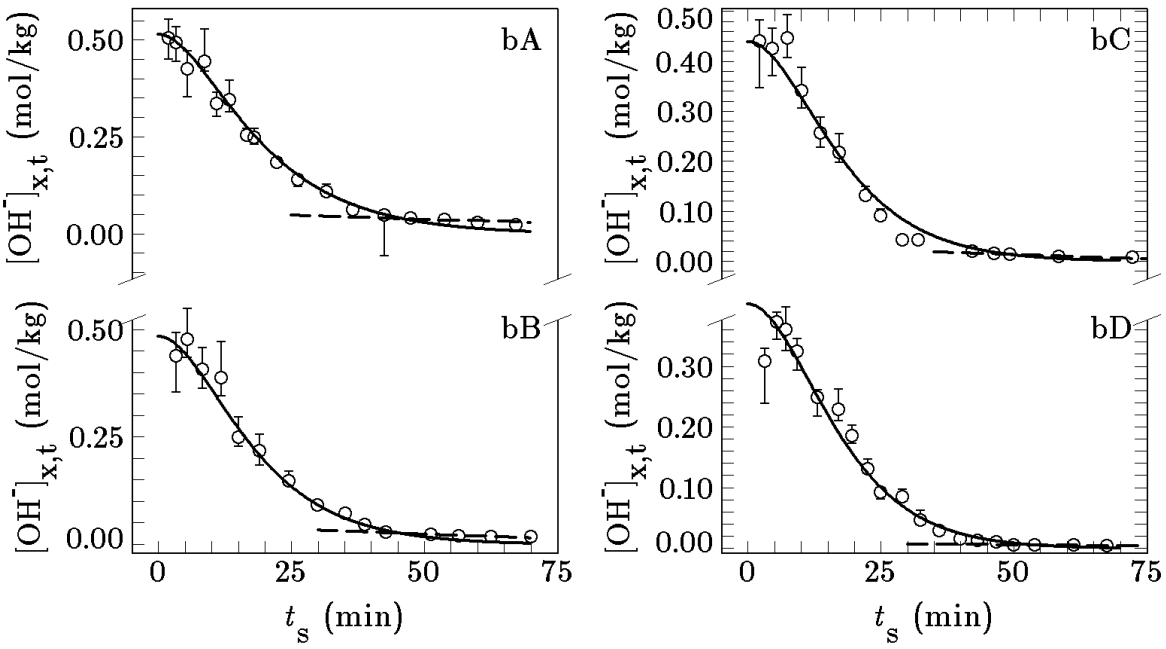

Figure 5b Changes in the molality concentrations, $[OH^-]_{x,t}$ of the OH^- ions during preparation and aging of the IM-HmRMs with x = 0.35 (bA), 0.5 (bB), 0.75 (bC) and 1.0 (bD). The IM-HmRMs were prepared by the *rt* stirring of the reaction mixtures having the starting chemical compositions: xTEOS:0.25TPAOH:20H_2O. The values of $[OH^-]_{x,t}$, characterized by symbol ○, are determined (calculated) from the corresponding measured and corrected pH values (see SI-2) and the values of $[OH^-]_{x,t}$, characterized by solid curves, are calculated by simultaneous numerical solutions of the equations (1) and (2). t_s is the time of aging (with stirring), passed from the mixing of TEOS and TPAOH solutions (see Experimental methods).

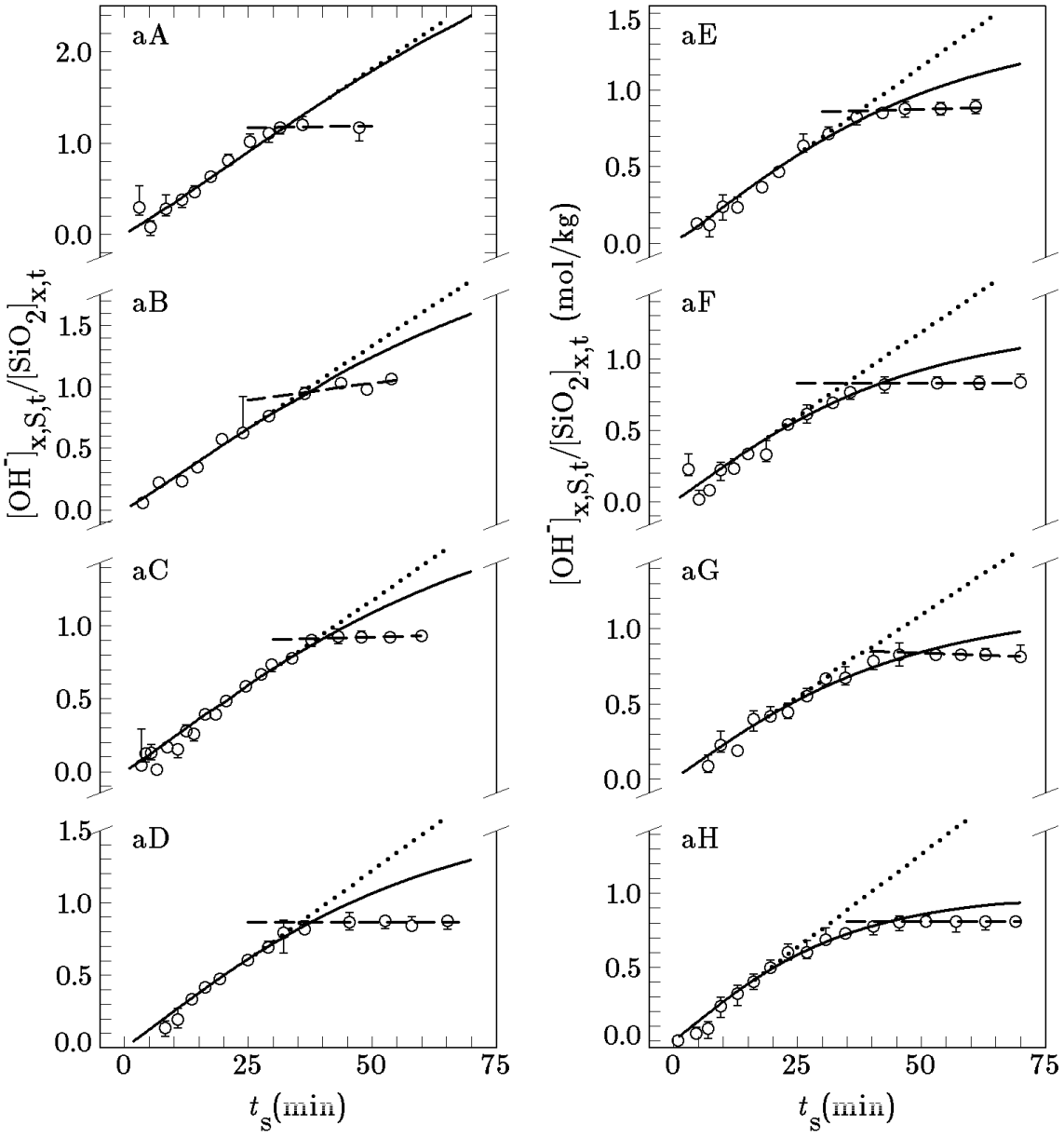

Figure 6a Changes of the calculated (solid curves) and measured (symbol ○) ratios $[OH^-]_{x,S,t}/[SiO_2]_{x,t}$ during preparation and aging of the IM-HmRMs with x = 0.05 (aA), 0.1 (aB), 0.125 (aC), 0.15 (aD), 0.175 (aE), 0.2 (aF), 0.22 (aG) and 0.25 (aH). The IM-HmRMs were prepared by the *rt* stirring of the reaction mixtures having the starting chemical compositions: xTEOS:0.25TPAOH:20H_2O. t_s is the time of stirring (aging) passed from the mixing of TEOS and TPAOH solutions (see Experimental methods).

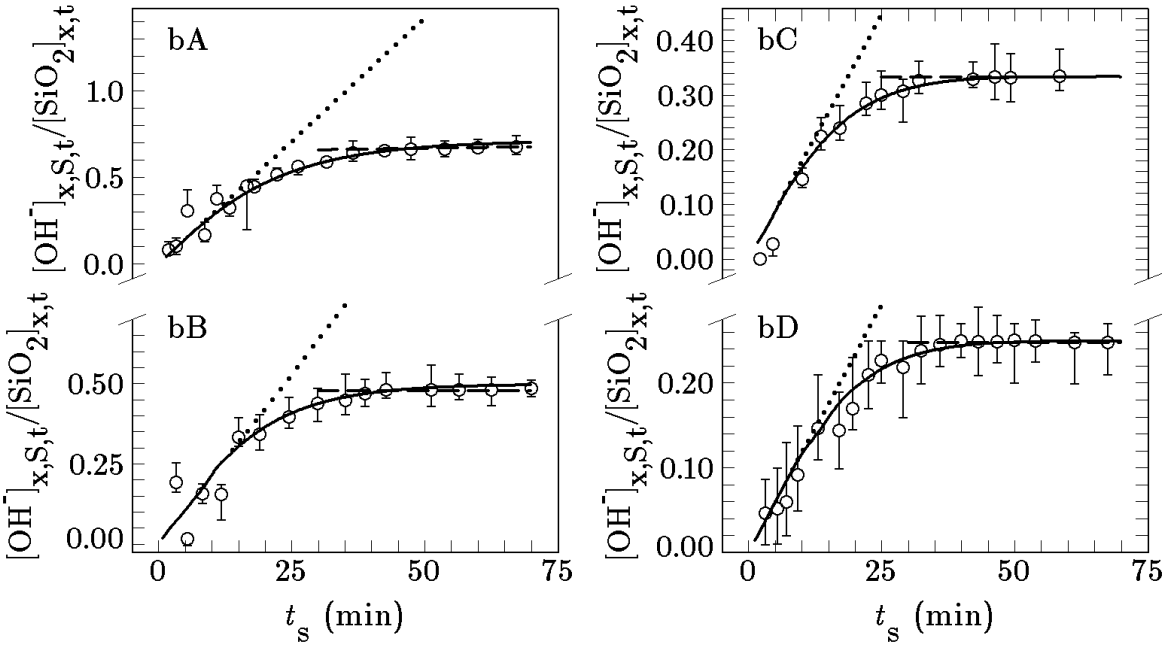

Figure 6b Changes of the calculated (solid curves) and measured (symbol ○) ratios $[OH^-]_{x,S,t}/[SiO_2]_{x,t}$ during preparation and aging of the IM-HmRMs with x = 0.35 (bA), 0.5 (bB), 0.75 (bC) and 1.0 (bD). The IM-HmRMs were prepared by the *rt* stirring of the reaction mixtures having the starting chemical compositions: xTEOS:0.25TPAOH:20H_2O. t_s is the time of stirring (aging) passed from the mixing of TEOS and TPAOH solutions (see Experimental methods).

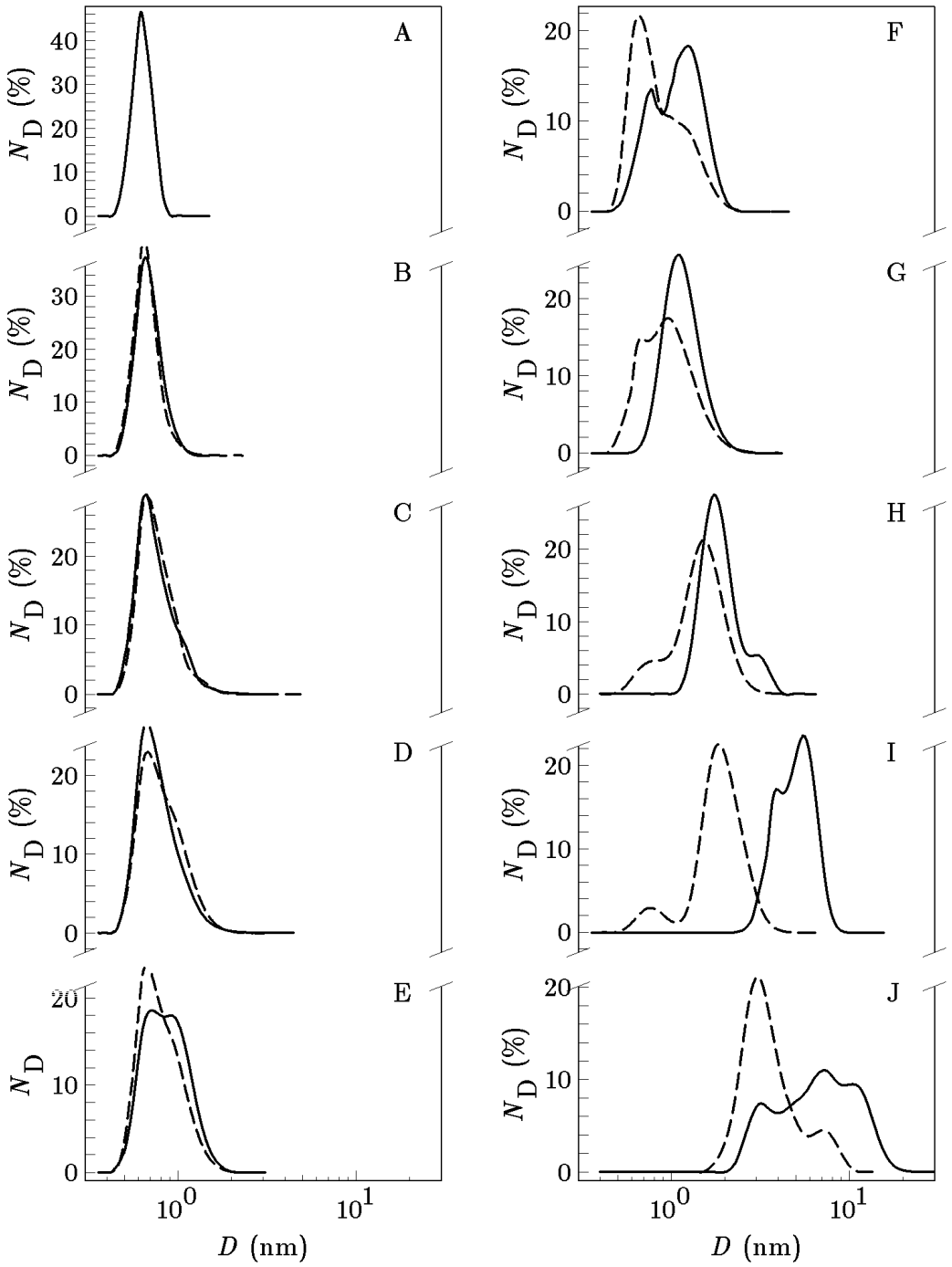

Figure 7 DLS-PSD curves by number measured in homogenous reaction mixtures (clear solutions) obtained by room-temperature stirring for t_s = 3 h (solid curves) and then by additional room-temperature aging for t_a = 21 h under static conditions (t_s + t_a = 24 h, dashed curves) of the IM-HmRMs having the starting chemical compositions: xTEOS:0.25TPAOH:20H_2O, with x = 0 (A), x = 0.05 (B), x = 0.2 (C), x = 0.25 (D), x = 0.275 (E), x = 0.35 (F), x = 0.5 (G), x = 0.65 (H), x = 0.75 (I) and x = 1 (J). N_D is the number percentage of the particles having the spherical equivalent diameter D.

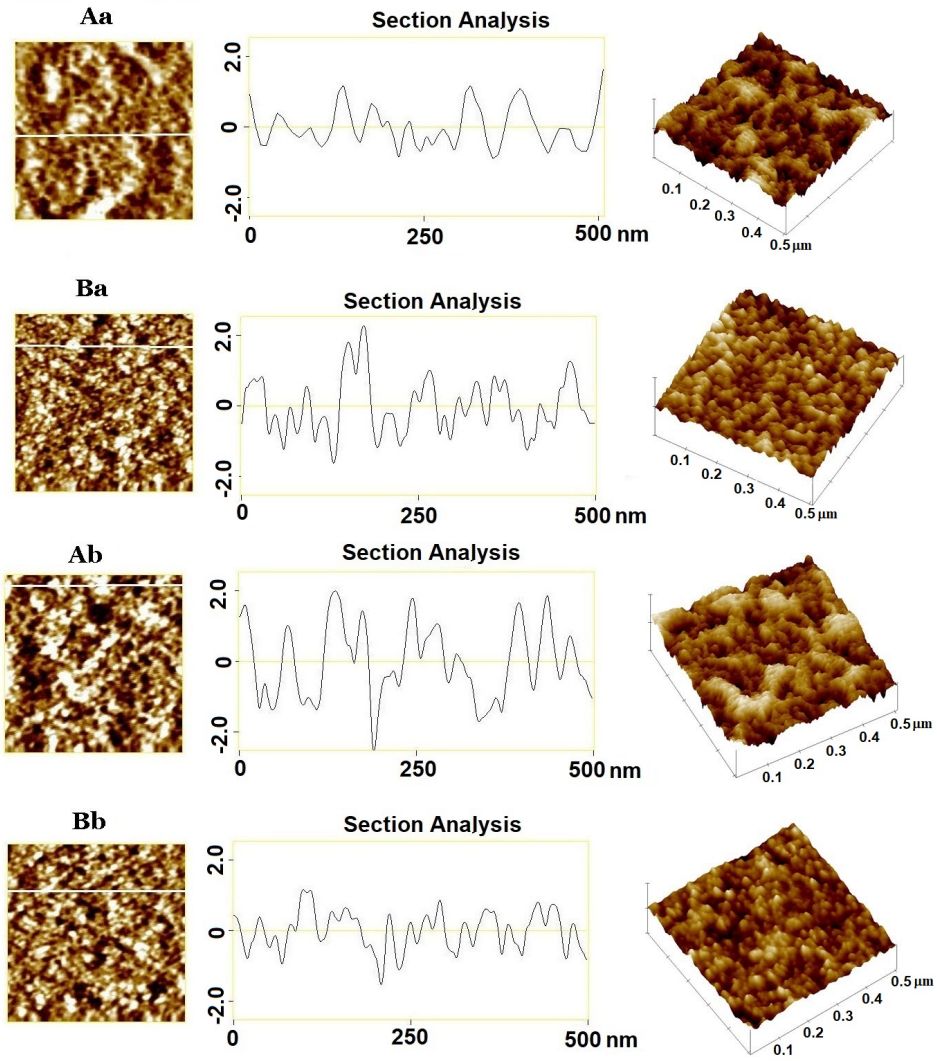

Figure 8 AFM topographic images and corresponding cross-section analyzes of the nanoparticles formed during room-temperature stirring for t_s = 3 h (Aa, Ba) and then by additional room-temperature aging for t_a = 21 h under static conditions; $t_s + t_a$ = 24 h (Ab, Bb) of the IM-HmRMs having the starting chemical compositions: xTEOS:0.25TPAOH:20H_2O, with x = 0.1 (Aa, Ab) and x = 0.2 (Ba, Bb). Images are presented as 2D height data (left), the cross-section through the line shown on the same scale: scan size of 500 nm × 500 nm and vertical scale of 5 nm (middle) and as 3D height data are shown on the same scale: scan size 500 nm × 500 nm and vertical scale of 5 nm (right)

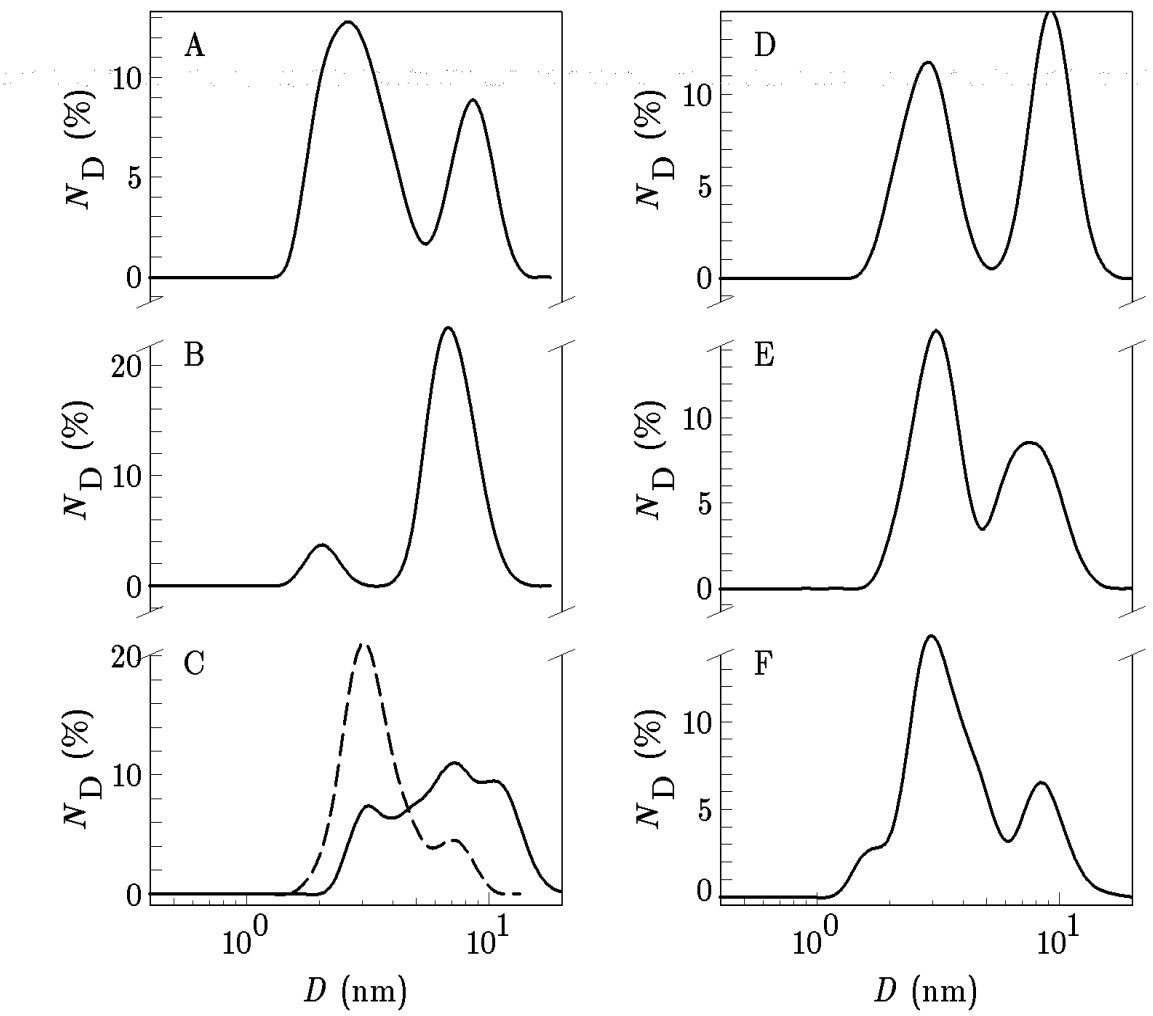

Figure 9 The size distributions by number (solid curves) of the nanoparticles formed during the room-temperature stirring for t_s = 2 h (A), 2.5 h (B), 3 h (C), 3.5 (D), 4.5 h (E) and 6 h (F), of the IM-HmRM having the starting chemical compositions: 1TEOS:0.25TPAOH:20H_2O. The dashed curve in the part (C) represent the size distribution of the particles obtained in the same IM-HmRM stirred at room temperature for t_s = 3 h and then, by additional room-temperature aging, under static conditions, for t_a = 21 h. N_D is the number percentage of the particles having the spherical equivalent diameter D.

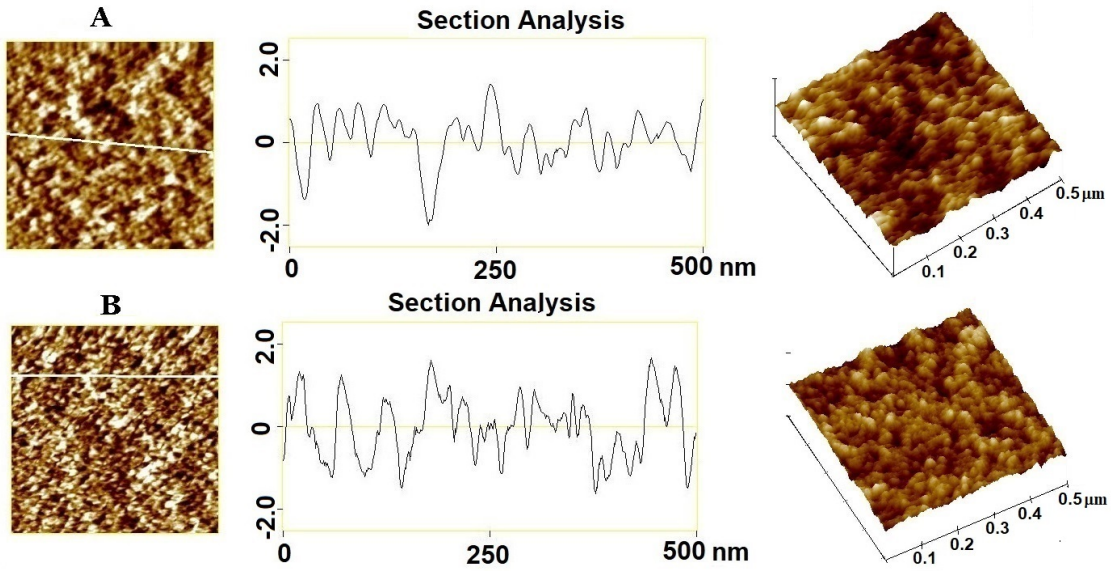

Figure 10 AFM topographic images and corresponding cross section analyzes of the nanoparticles formed during room-temperature stirring for t_s = 3 h (A) and then by additional room-temperature aging for t_a = 21 h under static conditions; $t_s + t_a$ = 24 h (B) of the homogeneous reaction mixture having the starting chemical composition: 1TEOS:0.25TPAOH:20H_2O. Images are presented as 2D height data (left), the cross-sections through the line are shown on the same scale: scan size of 500 nm × 500 nm and vertical scale of 5 nm (middle) and as 3D height data and are shown on the same scale: scan size of 500 nm × 500 nm and vertical scale of 10 nm (right).

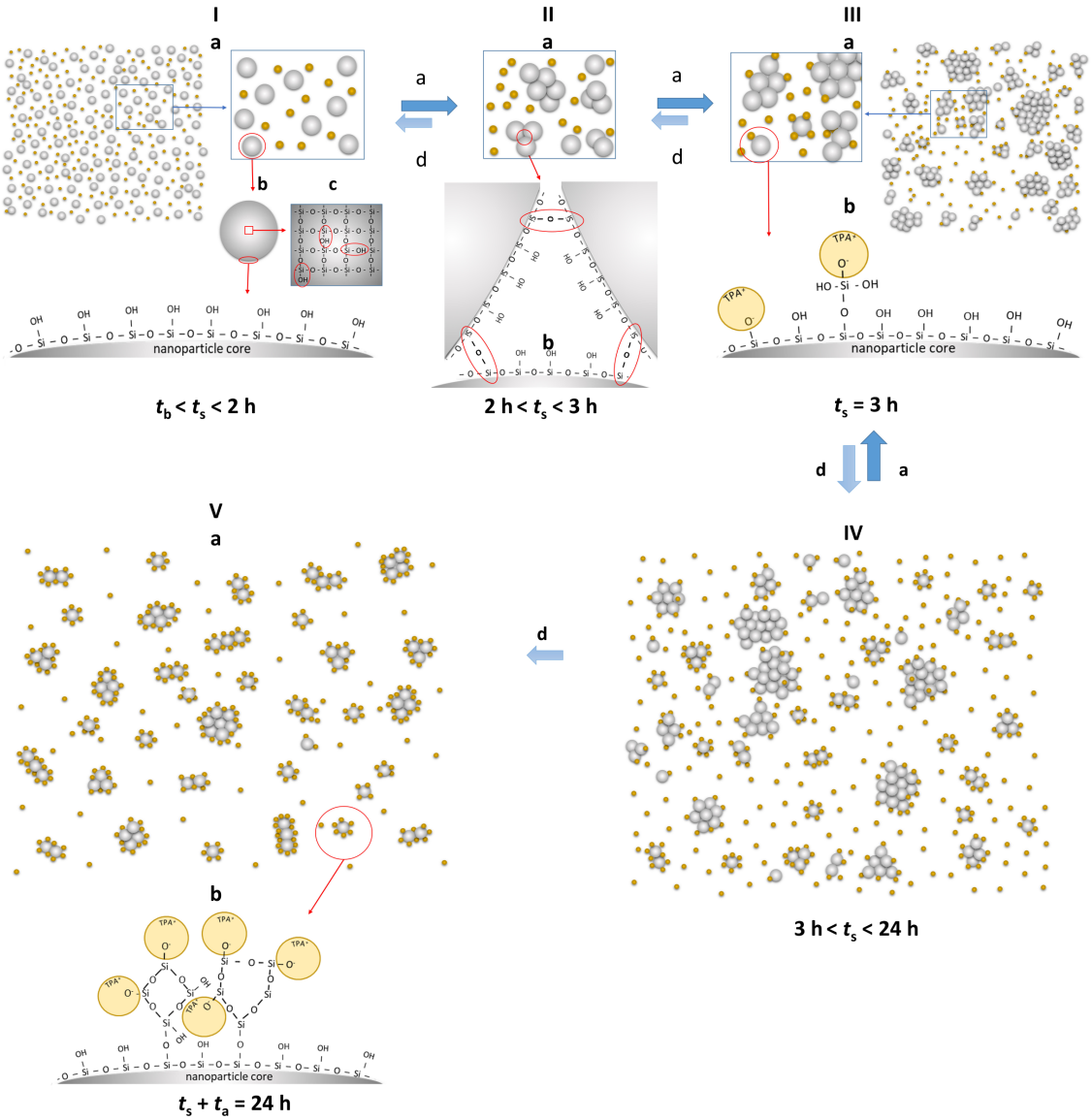

Scheme 1. Schematic presentation of the processes occurring in the HmRM having the starting chemical compositions: xTEOS:025TPAOH:20H_2O (x > 0.25; above the CAC) during room-temperature stirring/aging. The details are described in the text.

Remarks: (1) For practical reason, only the silica cores (larger gray spheres) and TPA^+-bearing oligomers (red spots) are presented. (2) For practical reason, all the TPA^+-bearing oligomers are presented by the spots of the same size.

Table 1 Influence of the mole fraction, x, of TEOS in the homogeneous reaction mixtures, having the starting chemical compositions: xTEOS:0.25TPAOH:20H_2O, on the molality concentrations, $[SiO_2]_{x,tot}$ = $[TEOS]_{x,0}$,$[OH^-]_{x,0}$, $[OH^-]_{x,S,b}$ and $[OH^-]_{x,S,24h}$ and the times t_{eq} and t_b. The definitions of $[SiO_2]_{x,tot}$, $[OH^-]_{x,0}$, $[OH^-]_{x,S,b}$, $[OH^-]_{x,S,24h}$, t_{eq} and t_b are explained in the text and omitted here for clarity reasons.

x	$[SiO_2]_{x,tot}$ (mol/kg)	$[OH^-]_{x,0}$ (mol/kg)	t_{eq} (min)	t_b (min)	$[OH^-]_{x,S,b}$ (mol/kg)	$[OH^-]_{x,S,24h}$ (mol/kg)
0.05	0.1186	0.5931	≈ 31	32.5	0.1230±0.0105	0.1306±0.0085
0.1	0.2315	0.5787	≈ 35	36	0.2037±0.0188	0.2362±0.0150
0.125	0.2859	0.5718	≈ 40	41	0.2488±0.0230	0.2618±0.0157
0.15	0.3391	0.5651	≈ 40	39	0.2841±0.0117	0.3126±0.0095
0.175	0.3910	0.5585	≈ 45	42.5	0.3185±0.0249	0.3535±0.0123
0.2	0.4416	0.5521	≈ 43	43.5	0.3824±0.0113	0.3896±0.0074
0.22	0.4814	0.5471	≈ 50	51	0.4010±0.0039	0.4246±0.0029
0.25	0.5397	0.5397	≈ 50	46	0.4277±0.0053	0.4747±0.0022
0.35	0.7230	0.5165	-	45	0.4660±0.0038	0.4765±0.0026
0.5	0.9703	0.4851	≈ 55	46	0.4555±0.0023	0.4601±0.0017
0.75	1.3220	0.4406	-	51	0.4256±0.0018	0.4281±0.0011
1.0	1.6140	0.4036	≈ 75	52	0.3975±0.0008	0.3986±0.0006

- The values of t_{eq} and t_b can vary from 2 – 6 min regardless to the value of x.

TOC Graphic

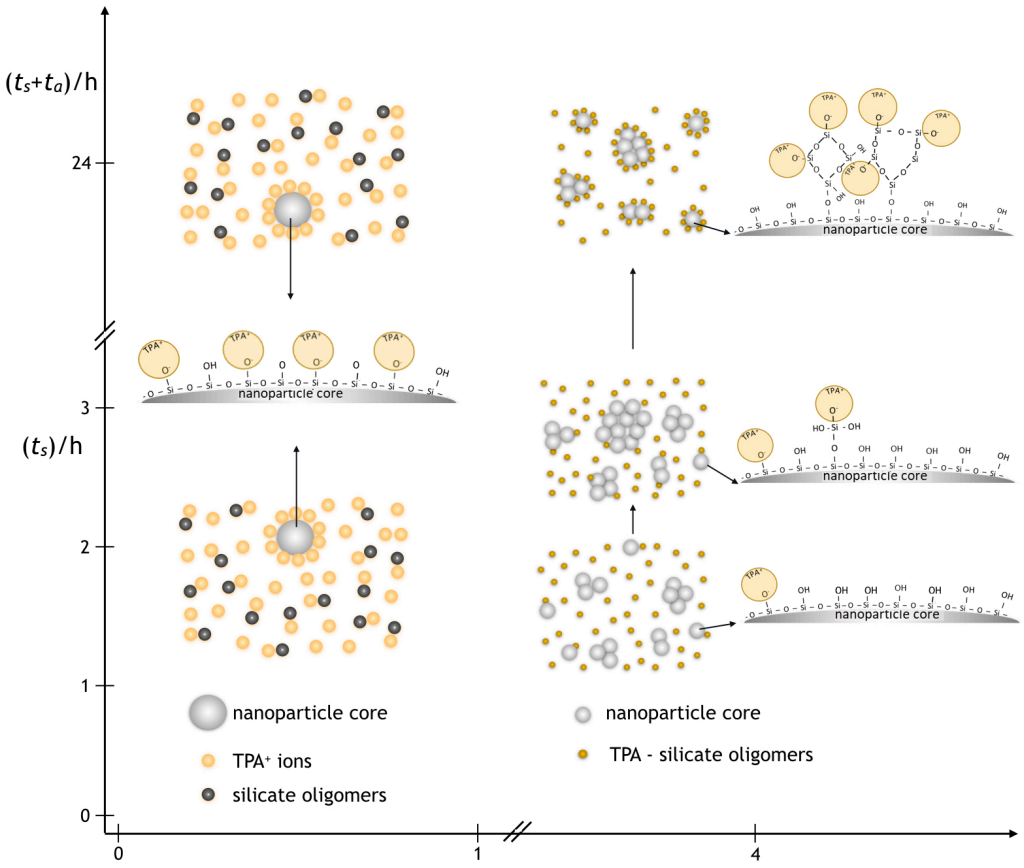

below the CAC ← $[SiO_2]/[OH^-]$ → above the CAC